The Connections of Layer 4 Subdivisions in the Primary Visual Cortex (V1) of the Owl Monkey

Jamie D. Boyd[1], Julia A. Mavity-Hudson[1] and Vivien A. Casagrande[1,2,3]

Departments of [1]Cell Biology, [2]Psychology and [3]Ophthalmology and Visual Sciences, Vanderbilt University, Nashville, TN 37232, USA

The primary visual cortex (V1) of primates receives signals from parallel lateral geniculate nucleus (LGN) channels. These signals are utilized by the laminar and compartmental [i.e. cytochrome oxidase (CO) blob and interblob] circuitry of V1 to synthesize new output pathways appropriate for the next steps of analysis. Within this framework, this study had two objectives: (i) to analyze the connections between primary input and output layers and compartments of V1; and (ii) to determine differences in connection patterns that might be related to species differences in physiological properties in an effort to link specific pathways to visual functions. In this study we examined the intrinsic interlaminar connections of V1 in the owl monkey, a nocturnal New World monkey, with a special emphasis on the projections from layer 4 to layer 3. Interlaminar connections were labeled via small iontophoretic or pressure injections of tracers [horseradish peroxidase, biocytin, biotinylated dextrine amine (BDA) or cholera toxin subunit B conjugated to colloidal gold particles]. Our most significant finding was that layer 4 (4C of Brodmann) can be divided into three tiers based upon projections to the superficial layers. Specifically, we find that 4α (4Cα), 4β (4Cβ) and 4ctr send primary projections to layers 3C (4B), 3Bβ (4A) and 3Bα (3B), respectively. Examination of laminar structure with Nissl staining supports a tripartite organization of layer 4. The cortical output layer above layer 3Bα (3B) (e.g. layer 3A) does not appear to receive any direct connections from layer 4 but receives heavy input from layers 3Bα (3B) and 3C (4B). Some connectional differences also were observed between the subdivisions of layer 3 and the infragranular layers. No consistent differences in connections were observed that distinguished CO blobs from interblobs or that could be correlated with differences in visual lifestyle (nocturnal versus diurnal) when compared with connectional data in other primates. Re-examination of data from previous studies in squirrel and macaque monkeys suggests that the tripartite organization of layer 4 and the unique projection pattern of layer 4ctr are not restricted to owl monkeys, but are common to a number of primate species.

Introduction

As originally pointed out by Zeki and Shipp (Zeki and Shipp, 1988), part of the function of V1 can be seen as combining disparate inputs from the lateral geniculate nucleus (Hubel and Wiesel, 1972; Livingstone and Hubel, 1982; Blasdel and Lund, 1983; Fitzpatrick *et al.*, 1983; Weber *et al.*, 1983; Diamond *et al.*, 1985; Lachica and Casagrande, 1992; Ding and Casagrande, 1997) in different ways to synthesize distinct classes of outputs (Zeki, 1978; Rockland and Pandya, 1979; Cusick and Kaas, 1988; Casagrande and Kaas, 1994). Because the different classes of inputs and outputs are often segregated into different layers and columns of V1 (reviewed in Casagrande and Kaas,1994), studying the connectivity between different layers of V1 can provide insights into how V1 generates its outputs.

Previous studies of interlaminar connections in V1 of various primate species have found that different sublayers of layer 3 receive inputs from different sublayers of layer 4 (4C). Note that a modification of the layering scheme of Hässler (Hässler, 1967) is used in the present paper since it can be applied across primate species [for discussion see (Casagrande and Kaas, 1994)]. Brodmann's layers (Brodmann, 1909) are given in parentheses. At the level of single cells, Golgi studies (Valverde, 1971; Lund and Boothe, 1975) and intracellular filling (Katz, 1989; Anderson *et al.*, 1993; Callaway and Wiser, 1996) showed that while neurons of layer 4α (4Cα) project primarily to layer 3C (4B) and to a lesser extent 3B, the neurons of layer 4β (4Cβ) have the opposite pattern, making many more terminations in layer 3B than in 3C (4B). Studies using small injections of tracer substances confined to particular sublayers of layer 3 have confirmed these findings at the population level (Lachica *et al.*, 1992, 1993; Yoshioka *et al.*, 1994). Thus, injections into layer 3C (4B) preferentially label cells in layer 4α (4Cα), while injections into layer 3B label cells in 4β (4Cβ) in addition to cells in 4α (4Cα). Layer 3A does not receive direct projections from layer 4 (4C), and thus is at least one step further removed from LGN inputs when compared with layers 3B and 3C (4B).

Although the connections of layer 4 described above have been most thoroughly documented in the Old World macaque monkey, similar patterns of connections, with some species differences, have been seen in the New World squirrel monkey and in the prosimian bushbaby (Lachica *et al.*, 1993). The species differences in the connection patterns between layers are illuminating, in that differences in connectivity may be related to species differences in physiological properties, providing a link between particular pathways and visual functions. For example, in some primate species, layer 3B has been divided into an upper portion, 3Bα (3B), and a lower portion, 3Bβ (4A). The lower subdivision is marked by a distinct LGN input from the P layers (Hubel and Wiesel, 1972; Hendrickson *et al.*, 1978), which shows as a thin dark line in a CO stain (Horton and Hubel, 1981; Hendrickson, 1985). In macaque monkeys, this layer receives a strong, focused projection from layer 4β (4Cβ) (Blasdel *et al.*, 1985). All three of these interconnected structures, from the P layers of the LGN, through layer 4β (4Cβ) and into layer 3Bβ (4A), show physiological evidence of being involved in processing color information (Blasdel and Fitzpatrick, 1984). In some primates, such as owl monkeys and bushbabies, the geniculate input to layer 3Bβ (4A) is lacking (Kaas *et al.*, 1976; Diamond *et al.*, 1985). Given that owl monkeys and bushbabies have only a single cone type (Wikler and Rakic, 1990; Jacobs *et al.*, 1993, 1996), one speculation is that LGN input to 3Bβ (4A) is related to color vision. Thus, interlaminar connections of layer 3B in the New World owl monkey might be different than those in other closely related primate species such as squirrel monkey.

Some later studies of interlaminar connections examined the differences in connectivity between CO blob and interblob columns in V1 (Lachica *et al.*, 1992, 1993; Yoshioka *et al.*, 1994;

Callaway and Wiser, 1996; Yabuta and Callaway, 1998). Comparisons among different species found that interlaminar connections of CO blobs and interblobs varied in ways that correlated with visual niche differences (Lachica *et al.*, 1993). Data on interlaminar connections in the owl monkey would allow comparisons of the patterns of connectivity between primates with a similar visual niche but different phylogeny (owl monkey and bushbaby) and between primates that are more closely related but differ in visual niche (owl monkey and squirrel monkey).

The analysis of interlaminar connections in the owl monkey V1 reported here did not reveal dramatic differences between the connections of 3B blobs and interblobs. What these data on interlaminar connections in the owl monkey did show was that the center part of layer 4 should be considered a separate sublayer (4ctr), with a unique pattern of connections compared with 4α (4Cα) and 4β (4Cβ). As discussed in this paper, layer 4ctr could be present in other primate species (Yoshioka *et al.*, 1994) as well as in the owl monkey, and not recognizing it may have led to errors of interpretation in previous studies which placed data on connections of three anatomical subdivisions into two conceptual compartments. An abstract of some of these results has been previously published (Casagrande *et al.*, 1992).

Materials and Methods

A total of 12 owl monkeys (*Aotus trivirgatus*) were used in this study. Prior to surgery, atropine sulfate (0.1 mg/kg) was given to inhibit salivation. Animals then were anesthetized deeply either with a combination of ketamine (20 mg/kg) and xylazine (2 mg/kg), or with isofluorane (vaporizer setting between 1.5 and 2.5% with fresh gas flow rates of 1 l/min). Throughout surgery heart and respiration rates were monitored and body temperature was maintained with a heating pad. Under sterile conditions, cortical injections were made into layers 3 and 4 of V1 using a stereotaxic instrument at depths established from prior studies (Lachica *et al.*, 1992, 1993). Postsurgical care included the administration of a long-acting antibiotic (Flocillin; Fort Dodge Laboratories, Fort Dodge, IA; 15 000 units/kg) every 24 h, and an analgesic (Banamine; Fort Dodge Laboratories; 1 mg/kg) given postsurgically and repeated as needed. Animals were carefully monitored until they were fully awake and able to eat and drink normally. Surgical procedures and animal care followed NIH guidelines and approval of the Vanderbilt University Institutional Animal Care and Use Committee.

Four different tracers were used to determine the distribution pattern of cells projecting to the subdivisions of layer 3. The tracers were horseradish peroxidase (HRP, Boehringer Mannheim-Grade I or Sigma-Type IX; Boehringer Mannheim, Indianapolis, IA and Sigma, St Louis, MO respectively), biocytin (Sigma or Molecular Probes, Eugene, OR), cholera toxin subunit B conjugated to 7 nm colloidal gold particles (CTB-Au; List Biologicals, Campbell, CA), or biotinylated dextran (10 000 mol. wt; Molecular Probes). Six to 10 injections were made in each hemisphere spaced at least 2 mm apart. Survival times were ~24 h for HRP and biocytin and 1 week for the CTB-Au and dextran.

For the HRP injections, 10% HRP was dissolved in physiological saline; in one case 0.1% polyornithine was added. This solution was injected iontophoretically with a 10–20 μm inner tip diameter glass pipette, using 1 μA positive current for 3 min. For the biocytin injections, 5% biocytin was dissolved in either saline (pH 7.4) or 0.05 M Tris buffer (pH 8.2). The biocytin was injected iontophoretically, 7 s on, 7 s off, for 1–15 min at 0.5–5 μA using a glass pipette with an inner tip diameter of 10–30 μm (Lachica *et al.*, 1991). The dextran and CTB-Au (~0.2 μl per injection) were pressure injected. Dextran and CTB-Au were dissolved in saline (pH 7.4) at a concentration of 10 and 1%, respectively.

Animals were euthanized with an overdose of sodium pentobarbitol. In all except one case, the animals were then perfused transcardially with saline or Ringer's lactate, followed by a solution of 3–4% paraformaldehyde. In one case we added 0.1% glutaraldehyde and 0.2% v/v of saturated picric acid. Brains were removed and cryoprotected by equilibrating in 30% sucrose in phosphate buffer overnight.

Frozen sections 40–60 μm thick were cut in the parasagital plane on a sliding microtome and collected in PBS. HRP labeled cells were visualized using a standard DAB reaction with 0.05% diaminobenzidine tetrahydrochloride (DAB, Sigma, D-5637) in PBS, 0.1 M phosphate buffer or Tris buffered saline (TBS) with 0.01% H_2O_2 added. Biocytin and dextran labeling were visualized using a Vector Standard Elite ABC kit (PK-6100), incubating for 1–2 h, then performing a DAB reaction as above. In some cases a variation of the DAB reaction was performed using 0.05 M imidazole, 0.6% nickel ammonium sulfate, 0.02% DAB and 0.0004% H_2O_2 (Tago *et al.*, 1987).

To silver enhance the CTB-Au reaction, the IntenSe M kit from Amersham was used. This reaction was further enhanced by adding additional silver (50–100 μl of a 2.0% solution of silver nitrate in 6 ml) to the solution from the Amersham kit.

In all cases, some sections were reacted for cytochrome oxidase (CO) in order to visualize the CO blobs. For the CO reaction, sections were transferred into a solution of 0.05% DAB, 0.03% cytochrome C (Sigma) and 0.02% catalase (Sigma) in either PBS, 0.1 M phosphate buffer or TBS, and reacted at 37°C until the blobs were clearly visible. In some sections, 0.06% nickel ammonium sulfate and 0.24% cobalt chloride were added for intensification of the stain, which substantially decreased the time of the reaction while allowing for greater differentiation of the blobs.

In some cases, sections were double labeled for both biocytin or BDA and CO. These sections were incubated in ABC as above, then transferred to the CO reaction solution without the addition of heavy metals. (Addition of metals in double-labeled sections created a very high background staining, making the labeled cells difficult to see.) When sections were sufficiently reacted, they were rinsed and placed into a solution of 0.05% DAB with 0.01% H_2O_2 and watched very carefully for the appearance of the labeled cells. In other cases the biocytin, HRP, CTB-Au or BDA reaction was completed before placing the sections into the CO reaction solution. When using the CTB-Au, better results were obtained when the CO was done before the silver intensification; however, it was found best to do an unintensified reaction for the CO, i.e. no nickel or cobalt, as the reagents in the Amersham kit removed the metals from the sections.

Injections were reconstructed using a camera lucida. Injection sites and CO blob locations were initially drawn at lower power (~×10) to help with alignment of sections. Final serial reconstructions were done at ×1200. After all sections were drawn, some sections that were single labeled for biocytin, HRP, CTB-Au or BDA were stained for cell morphology using cresyl violet in order to determine layer boundaries. These sections were photographed both with a dark blue filter (Wratten 47B), to block out the blue stained cells, and without a filter, giving alternate photographs of the same section to show both the labeled cells and cytoarchitecture. The positions of CO blobs were determined from either the adjacent CO stained sections or from sections that were double-labeled.

Results

In order to determine the general patterns of connections between the separate sublaminae of cortical layers 3 and 4 (4C), it was first necessary to establish a clear set of criteria for defining visual cortical layers. In the first section we describe how we defined cortical layers in V1 of the owl monkey. In the next four sections of the results we consider the connections of each of the subdivisions of layer 3, beginning with the most ventral sublayer, layer 3C (4B). Injections within CO blobs and interblobs were analyzed separately. In each case we used data from both large injections that could involve more than one sublayer or compartment and very restricted injections to test specific hypotheses about the patterns of connections. A primary projection was predicted to be present in all cases involving the targeted sublayer, whereas the variable presence of connections was interpreted in a number of ways depending upon the extent of the injection. In this way, small injections, which carry the possibility of false negatives from low labeling levels but have low probability of false positives, were com-

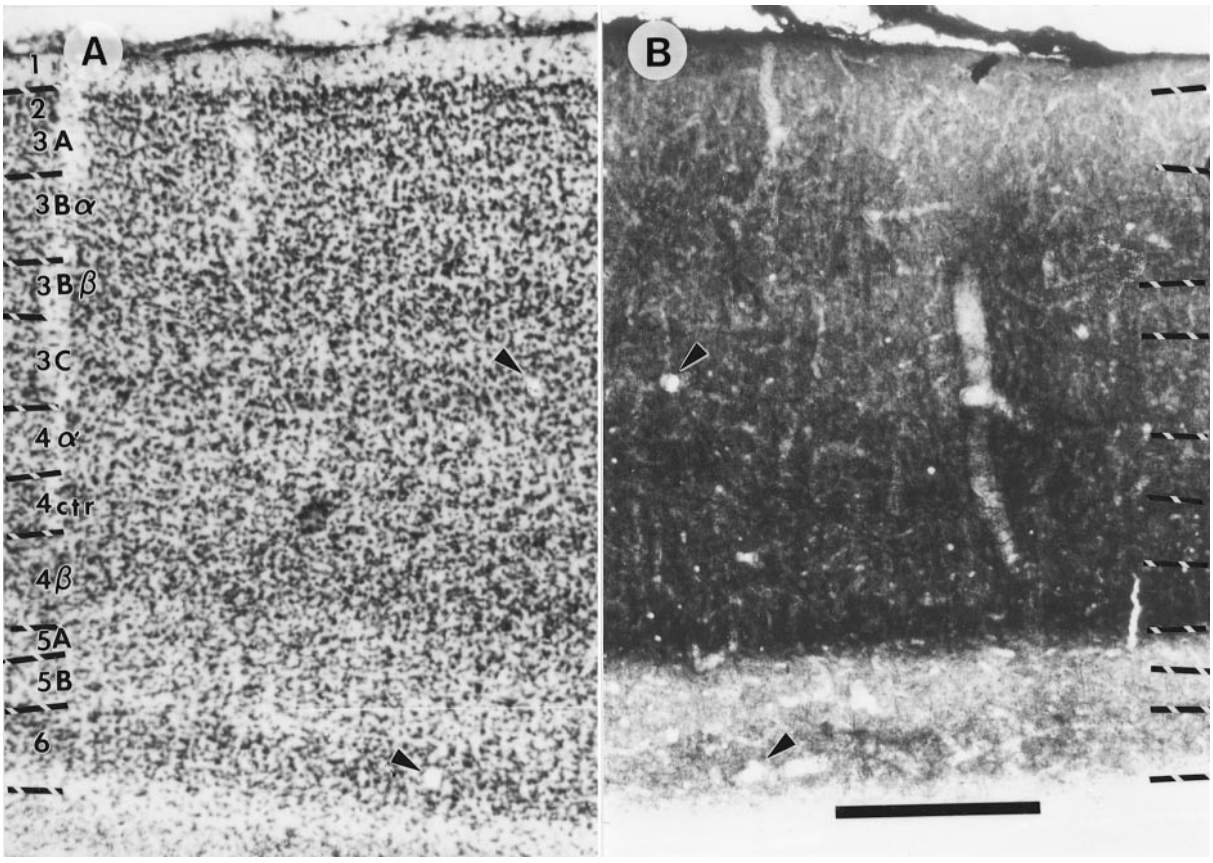

Figure 1. Lamination in owl monkey primary visual cortex (V1). (*A*) A photomicrograph of a Nissl stained coronal section with layers indicated in Arabic numerals. Note that we use a modification of Hässler's system to designate layers (Hässler, 1967). The key differences from the more commonly used nomenclature of Brodmann (Brodmann, 1909) are as follows with Brodmann's nomenclature in parentheses: 4 (4C), 3C (4B), 3Bβ (4A), 3Bα (3B). Based upon differences in connections, we divide layer 4 into three tiers, 4α (4Cα), 4ctr and 4β (4Cβ). (*B*) An adjacent section stained for CO. For ease of comparison, the CO section has been flipped so that it is a mirror image of the Nissl stained section. Common blood vessels in the two sections are marked with arrows. See text for details. Scale bar = 300 μm.

pared with larger injections, which carry the possibility of false positives from axons innervating adjacent cortical layers, but will have lower probabilities of false negatives.

Lamination of Owl Monkey V1

Figure 1 shows the lamination scheme used in this study. There are two main lamination schemes in use for primate visual cortex. In Hässler's scheme (Hässler, 1967), layer 4 corresponds to the main geniculate input layer, and cortical layers above this are designated as subdivisions of layer 3, unlike Brodmann's original lamination scheme (Brodmann, 1909) and its later modifications (Billings-Gagliardi *et al.*, 1974), where layer 4 is more extensive. In this paper we use a modification of Hässler's scheme that was used for the owl monkey originally by Diamond *et al.* (Diamond *et al.*, 1985). In the latter modification Brodmann's layer 4B becomes 3C, and 4A becomes 3Bβ. Throughout the paper we indicate Brodmann's layers in parentheses.

We consider layer 4(4C) to be composed of three tiers: a lower tier containing very small, closely packed cells that we call 4β (4Cβ); an upper tier, 4α (4Cα), with larger, more loosely packed cells; and a middle tier, where cell size and packing density are intermediate between those of 4β (4Cβ) and 4α (4Cα). In this paper, we have given the middle tier of layer 4 (4C) a separate designation, 4ctr, to highlight its distinctive intracortical and geniculocortical connections (see below). Also, note that a narrow, cell sparse cleft morphologically divides layer 4β (4Cβ) in the owl monkey (see Figure 1*A*) (Diamond *et al.*, 1985). Although this sublayer is not clearly demonstrable in Nissl staining in other primates, a similar sized band was noted using CO-staining in neonatal macaque monkeys (Horton, 1984; Blasdel *et al.*, 1985).

The subdivisions of layer 4 (4C) also can be seen in sections stained for CO in the adult owl monkey. Although all subdivisions of layer 4 (4C) stain darkly for CO, layer 4β (4Cβ) has slightly darker CO staining than layer 4ctr. In layer 4α (4Cα), patches of darker CO staining can be seen in register with the CO blobs in layer 3. These patches are darker than CO staining in layer 4ctr as well as darker than portions of layer 4α (4Cα) below interblobs.

Layer 3 in the owl monkey, as in other simian primates, can be divided into three distinct layers. Layer 3A is a relatively cell sparse layer under the narrow cell rich layer 2, while the cells of layer 3B are more closely packed than those in layer 3A. The border between layers 3A and 3B is often marked by a row of relatively large pyramidal cells. Although not noted in the study of Diamond *et al.* (Diamond *et al.*, 1985), it is apparent that layer 3B in the owl monkey, as in the squirrel monkey (Fitzpatrick *et al.*, 1983), can be subdivided based on the smaller size and increased packing density of neurons in the bottom part of the sublayer 3Bβ (4A) compared with the top part [3Bα (3B)]. In CO stained sections, the CO blobs are dense in layer 3Bα (3B) and are much lighter in 3A and 3Bβ (4A), so that these sublayers of

layer 3 are as well defined with CO as with Nissl staining. In well-stained sections reacted for CO, a thin band of staining can often be seen at the top of the cell sparse part of layer 3C (4B), at the base of layer 3Bβ (4A). This band of staining is at the same level as the thin band of CO staining in other primate species which colocalizes with a second zone of P geniculate input; this upper tier of geniculate input is lacking in the owl monkey (Kaas *et al.*, 1976; Ding and Casagrande, 1997). Layer 3C (4B) is composed of a lower subdivision containing large cells that project to the middle temporal (MT) visual area (Diamond *et al.*, 1985) and an upper, cell sparse subdivision.

Layer 5 is divisible into two sublayers, 5A and 5B. Sublayer 5A is composed of small, tightly packed cells and blends into layer 4β (4Cβ) such that it becomes difficult to distinguish the border between layers 4 and 5 using only a Nissl stain, although this border is very sharp in CO stained sections. The cells of layer 5B are larger and less tightly packed than those in layer 5A. Both sublayers of layer 5 are relatively pale in CO stained sections when compared with layers 4 and 6. Layer 6 is marked by closely packed cells and high levels of CO activity, making the border between layers 5 and 6 clear in both Nissl and CO stained sections.

Some of our injections of BDA that involved white matter labeled axons that were morphologically similar to previously described LGN axons. In some cases, individual axons respected the division of layer 4 (4C) into the three sublayers shown in the Nissl and CO stained sections. Figure 2 shows two low power photomicrographs of axons that terminate preferentially in 4α (4Cα) and 4β (4Cβ), leaving an afferent sparse cleft in the center of layer 4, 4ctr. The sections shown in Figure 2*B*,*C* were counterstained with Nissl or CO, respectively, showing that the afferent sparse gap corresponds to layer 4ctr as defined earlier. Although we found numerous axons that were confined to either layer 4α (4Cα) or 4β (4Cβ), we never found axons that were confined solely to layer 4ctr, although some axons had sparse branches in this sublayer. Perhaps 4ctr receives input from axons that branch in more than one sublayer. The view that this sublayer receives fewer afferents than 4α (4Cα) and 4β (4Cβ) is reinforced further by its relatively lighter CO staining.

As in our previous study (Lachica *et al.*, 1993), we used the pattern of connections to V2 to help define the sublayers of layer 3. Figure 3 shows two examples of patches of cells labeled from injections into V2. Cells in layers 3A and 3Bα (3B) both project to V2. The border between these two layers is demarcated by the size difference of the V2 projecting cells; those in 3Bα (3B) are distinctly larger than those in 3A. The cell size difference between 3A and 3Bα (3B) is easier to appreciate in cells labeled from V2 since more of the cell structure is visible than is evident in a Nissl stain. Note that cells in layer 3Bβ (4A) are distinct in that very few project to V2. This difference in V2 connectivity between 3Bα (3B) and 3Bβ (4A) supports the conclusion that these sublayers are distinct in the owl monkey even in the absence of the geniculate input to layer 3Bβ (4A) seen in other simian primates. Note that a previous study of the laminar location of V2-projecting neurons in macaque and squirrel monkey concluded that these cells were restricted to 3A (Rockland, 1992). It is clear, however, from the Nissl counterstained material (see Rockland's figure 3A,D) that the present study agrees with her results; the discrepancy is due to different assignments of laminar borders between the two studies. The pattern of connectivity with V2 also distinguishes layer 3A from layer 2, as cells in layer 2 do not project to V2. We were not able to study interlaminar connections of layer 2 separately from those of layer 3A, because all of the injections that included layer 3A also included portions of layer 2.

Connections of Layer 3C (4B)

A total of eight injections were made into layer 3C (4B). Of these injections, two were entirely restricted to layer 3C (4B), six were located below a CO blob and two below an interblob. Figure 4 shows an example of an injection of BDA that was made into layer 3C (4B) below a CO blob. Following 3C (4B) injections, labeled cells were found in all layers except layers 1, 2 and 4β (4Cβ); cells were found only rarely in layer 6. Within layer 4 (4C), cells were retrogradely labeled in both 4α (4Cα) and 4ctr. Figure 4*C* shows a higher power photomicrograph showing the labeled cells within these sublayers. Most of the retrogradely labeled cells exhibit a stellate morphology, although a minority of the labeled cells in the upper part of layer 4α (4Cα) were pyramidal cells, as shown by the apical dendrite in the cell marked by an arrow. Labeled cells with obvious apical dendrites were not found in layer 4ctr. Although not easily seen in these photomicrographs, cellular and terminal labeling was found in both layers 5A and 5B following injections in 3C (4B). Figure 4*D* shows a low power photomicrograph of an adjacent section double labeled for CO and for the BDA tracer. This section shows that the injection in this case was located beneath a CO blob.

Figure 5*A* shows a serial reconstruction of the labeling resulting from the 3C (4B) injection shown in Figure 4. In addition to showing the vertical labeling pattern, this figure also shows axons extending horizontally and terminating in layer 3C (4B) and 4α (4Cα) as much as several millimeters away from the injection site. Figure 5*B*,*C* shows two additional reconstructions from other injections into layer 3C (4B), one below an interblob and the other below a blob, respectively. In both of these cases, there were labeled cells in layers 4α (4Cα) and 4ctr. In the three injection reconstructions shown it appears that following injections located below interblobs more cells are labeled in 4ctr (Fig. 5*B*), whereas following injections below blobs (Fig. 5*A*,*C*) more cells are labeled within 4α (4Cα). However, these patterns were not consistent across cases.

Connections of Layer 3Bβ (4A)

A total of 17 injections were made into layer 3Bβ (4A), including three that were restricted to layer 3Bβ (4A). Ten were located below a CO blob, four below an interblob and three below blob/interblob borders. The connections of layer 3Bβ (4A) were of special interest because the owl monkey, unlike some other simian primates, lacks geniculate input to this layer (Kaas *et al.*, 1976). Figure 6 shows an example from one experiment involving an injection of biocytin in layer 3Bβ (4A) beneath a CO blob. The injection is quite small (<200 μm in diameter) and is centered in layer 3Bβ (4A). Because of the curvature of the cortex, labeling was not present in the section containing the injection, but was present in the following three sections. A small cluster of labeled cells was found in layer 4β (4Cβ). Two lightly labeled cells also were found in layer 4ctr; no labeled cells were found in layer 4α (4Cα). In layer 5, cells were labeled in layer 5A, but not layer 5B. The assignation of labeling to layer 5A was especially clear in cases where sections were counterstained with CO (not shown), as there was no gap between the bottom border of layer 4 and the labeled cells in layer 5. This pattern of labeling was consistent from case to case, and for injections below both blobs and interblobs, with the exception that in some cases a few labeled cells were also found in layer 5B.

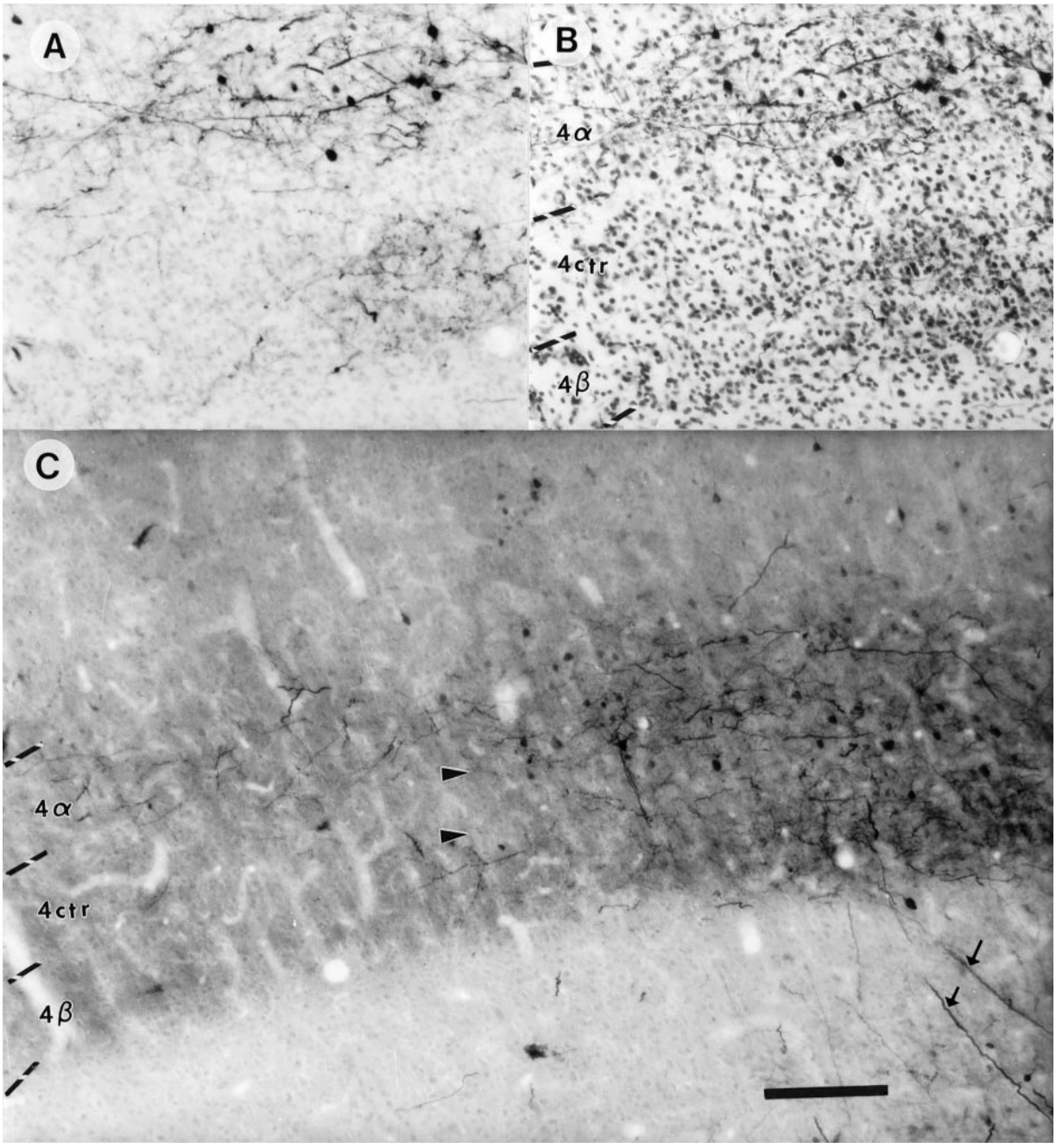

Figure 2. Very few LGN axons terminate within 4ctr as shown in these examples. (*A*,*B*) Photomicrographs of BDA-labeled axons in layer 4 taken with and without the blue filter, respectively. Note the paucity of terminals in layer 4ctr. Comparison with the Nissl staining visible in (*B*) shows that the gap in labeling corresponds to layer 4ctr. (*C*) An example of BDA labeling from a section also stained for CO. Note how the distribution of labeled fibers mirrors the density of the CO stain, and that layer 4ctr, as distinguished by lower density of CO staining, corresponds to the gap in labeling (between the arrowheads). The arrows mark axons ascending from injections in the white matter to terminate in layer 4. Scale bar = 150 μm.

Figure 7 shows examples of serial reconstructions of the label following layer 3Bβ (4A) injections. The injections shown in Figure 7*A*,*C* lie below CO blobs while the injection shown in Figure 7*B* lies below an interblob The reconstruction shown in Figure 7*A* is from the same experiment illustrated in Figure 6.

As shown in Figure 8, anterograde labeling from an injection centered in layer 4β (4Cβ) strengthened the conclusion that 4β (4Cβ) projects strongly to layer 3Bβ (4A). Figure 8*A* shows the injection site and labeling under dark-field optics, while Figure *8B* shows the same section stained for Nissl substance and viewed with bright-field optics to show the lamination. The injection site is mostly located in layer 4β (4Cβ), with some involvement of 4ctr. Anterogradely labeled fibers from this injection site can be seen ascending in the cortex and terminating in a tightly focused field in layer 3Bβ (4A). Further labeling in an adjacent section is shown in the dark-field/bright-field pair of photomicrographs shown in Figure 8*C*,*D*, respectively. Here, sparser, more broadly focused terminals can be seen extending

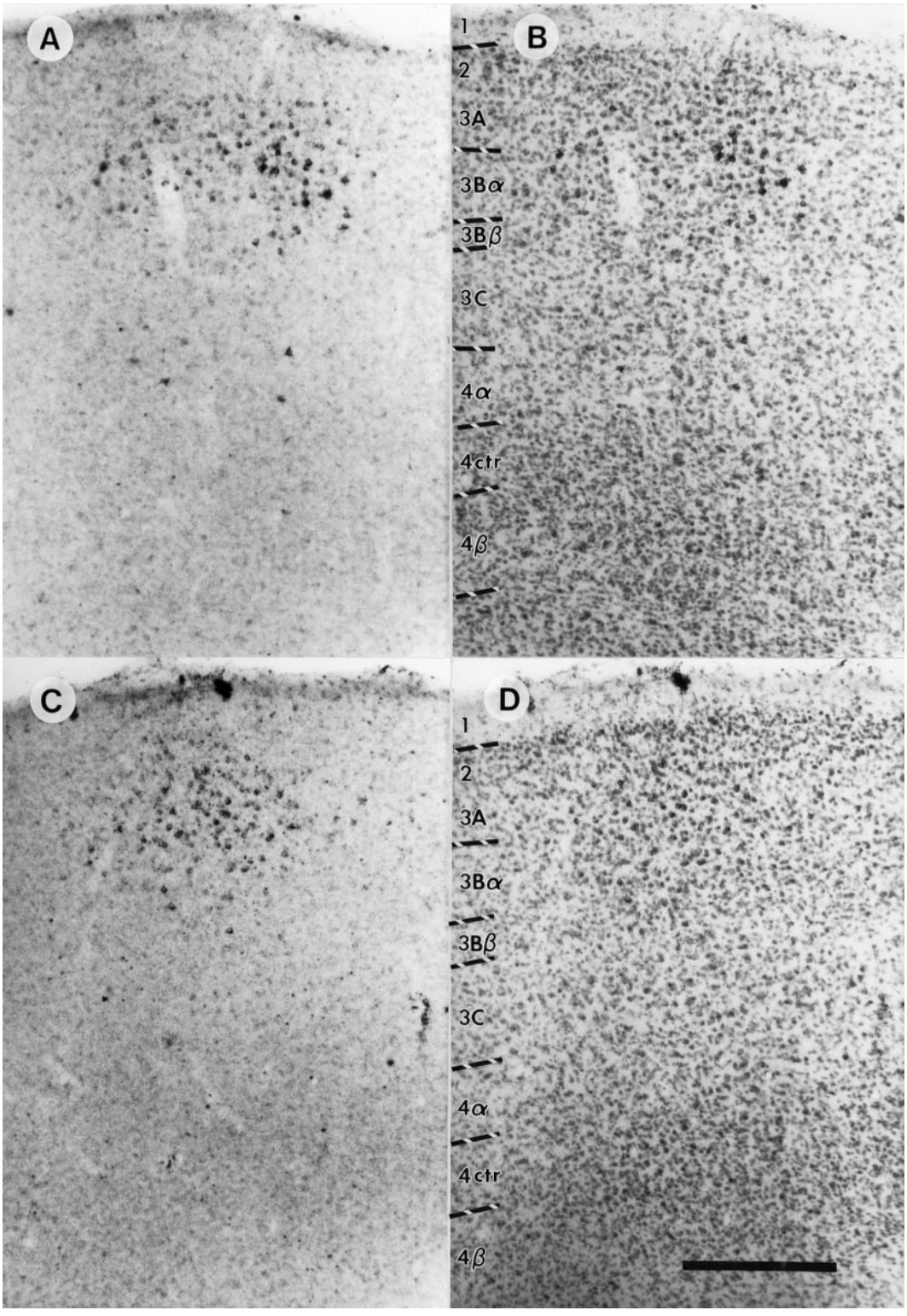

Figure 3. The distribution of V1 output cells projecting to area V2. (*A*,*C*) Cells labeled with CTB-Au from injections in V2. These cells are located mainly within layers 3A and 3Bα (3B). (*B*,*D*) The same sections as in *A* and *C*, respectively, only without the blue filter, in order to show the lamination. Layer 2 does not contain labeled cells, and layer 3Bβ (4A) contains very few labeled cells. Note that V2-projecting cells in layer 3Bα (3B) are larger than V2-projecting cells in 3A. Other conventions are as in Figure 1. Scale bar = 250 μm.

upwards into layer 3Bα (3B). It is possible that these sparse terminals were labeled either directly from 4β (4Cβ) or from neurons in 4ctr, as the injection site encroached on this sublayer.

Connections of Layer 3Bα (3B)

A total of 18 injections were made into layer 3Bα (3B), three of which were restricted to layer 3Bα (3B). Eleven were located in

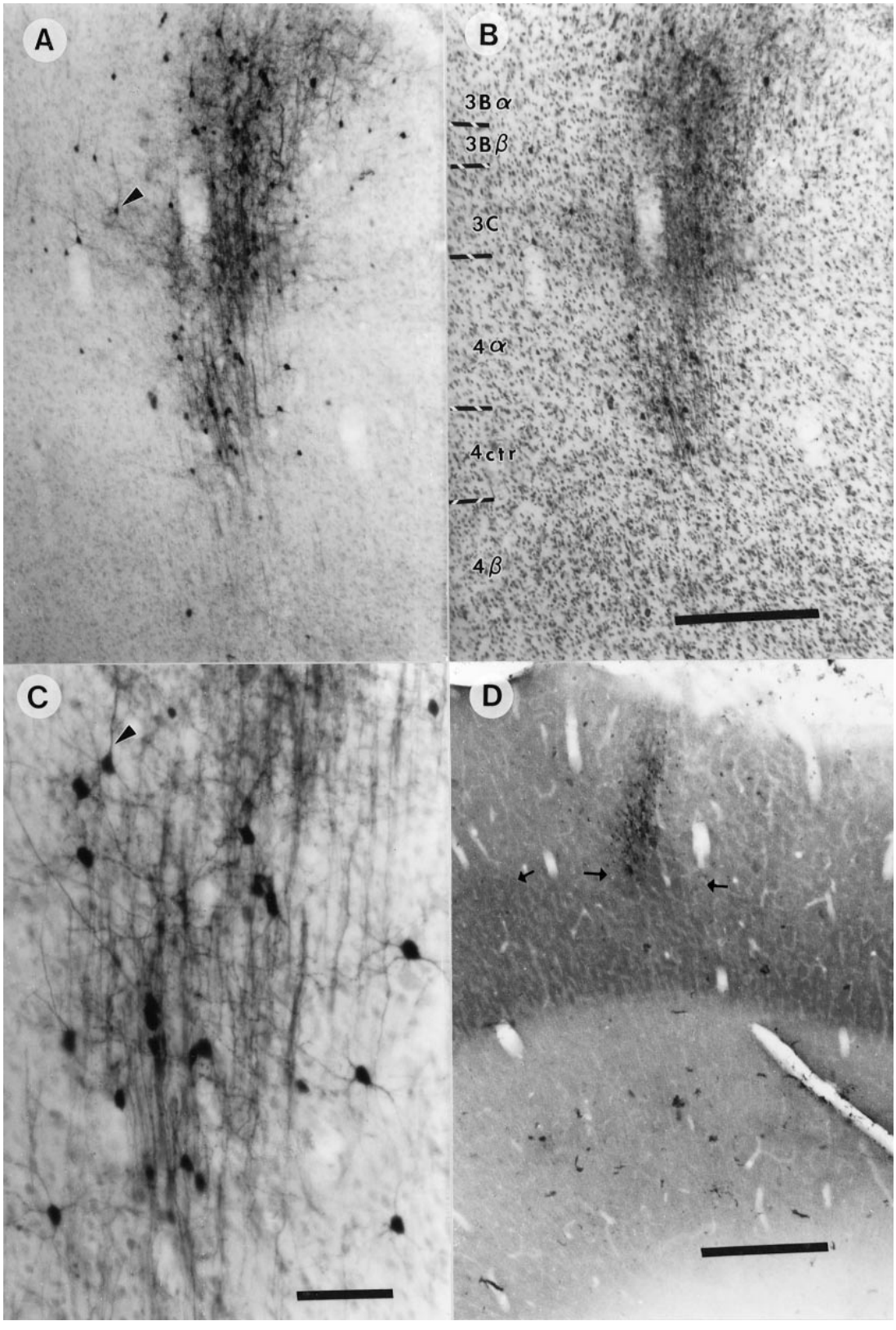

Figure 4. An example of one injection within layer 3C (4B) located beneath a CO blob. (*A*) The pattern of retrogradely labeled cells resulting from this BDA injection. See also the reconstruction of this injection in Figure 5*A*. (*B*) The same section as in (*A*) counterstained for Nissl substance to reveal the layers. (*C*) A higher magnification photomicrograph of the labeled cells shown in (*A*). Note that the labeled cells are located mainly with layer 4α (4Cα). The injection site location is shown on an adjacent CO counterstained section in (*D*). The location of the injection site in 3C (4B) is marked by arrows below the CO blob. The arrow to the left marks the edge of another blob column. The arrowheads in (*A*) and (*C*) mark apical dendrites of labeled pyramidal cells in layers 3C (4B) and 4α (4Cα) respectively. Scale bars: (*A*,*B*) = 200 μm, (*C*) = 75 μm, (*D*) = 400 μm.

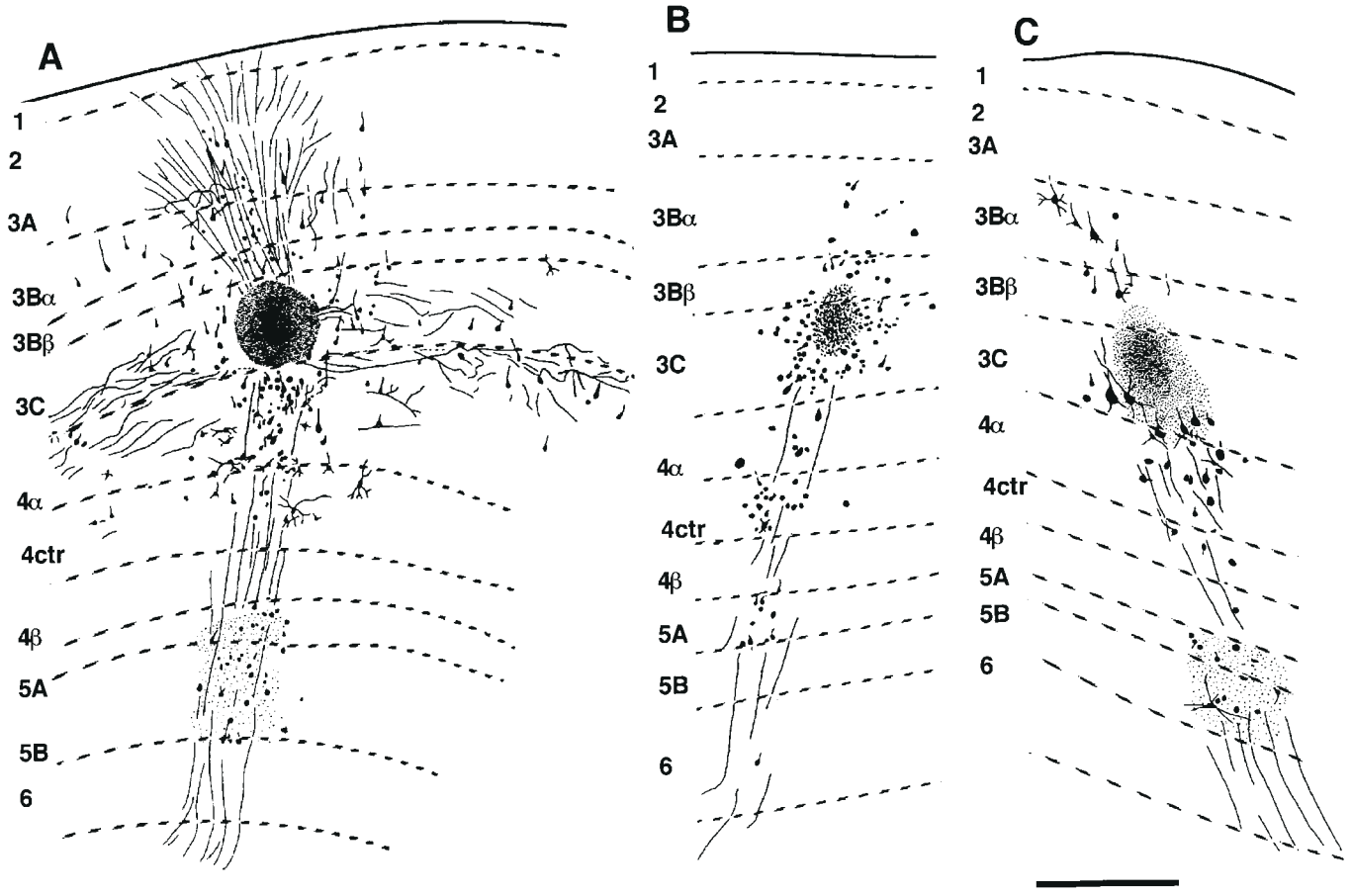

Figure 5. Reconstructions of the distribution of retrograde (large black dots) and anterograde (fine stipple) label following injections within layer 3C (4B). (*A*) A reconstruction of the label following the large 3C (4B) injection of BDA illustrated in Figure 4. Retrogradely labeled cells are found in all layers except layers 1, 2, 4β (4Cβ) and 6. (*B*) A reconstruction of a smaller 3C (4B) injection of biocytin located beneath an interblob. Retrogradely labeled cells are found mainly in 4α (4Cα), 4ctr and 5A. (*C*) A reconstruction of another 3C (4B) biocytin injection located beneath a CO blob. As in (*A*), most of the retrograde label is located within layer 4α (4Cα) and layer 5. Following all of these injections, anterograde and retrograde label was also seen extending tangentially within layer 3C (4B), although these projections were not reconstructed in (*B*) and (*C*). Cortical layers are indicated in Arabic numerals. Scale bar = 250 μm.

a CO blob, four in an interblob and three in both. The pattern of retrogradely labeled cells following injections into layer 3Bα (3B) was distinct from the pattern seen following injections within layer 3Bβ (4A). Unlike injections involving 3Bβ (4A), injections involving 3Bα (3B) always resulted in heavy retrograde filling of cells located within layer 4ctr. Figure 9 shows two examples of injections centered in 3Bα (3B). Figure 9*A*,*B* shows, respectively, a CTB-Au injection into layer 3Bα (3B) in a blob, photographed with the blue filter to show the labeling and without the filter to show the lamination. Figure 9*C*,*D* shows a similar pair of photomicrographs for an injection of HRP into layer 3Bα (3B) in an interblob. Although centered in layer 3Bα (3B), both of these injections encroached somewhat on layer 3Bβ (4A). In both cases the majority of labeled cells are seen in layer 4ctr.

Figure 10 shows reconstructions of three layer 3Bα (3B) injections. The injection centered within a blob shown in Figure 10*A* is the same as the one shown in Figure 9*C*,*D*, while the one shown in Figure 10*B* is the same as the one shown in Figure 9*A*,*B*. The other reconstruction shows a smaller injection centered within an interblob that avoided layer 3Bβ (4A) (Fig. 10*C*). In this case, labeled cells in layer 4 were fewer in number, but these labeled layer 4 cells were almost completely confined to layer 4ctr, with the exception that injections located within CO blobs always resulted in cells labeled in 4α (4Cα). These injections also resulted in dense retrograde and anterograde label within layer 3C and both subdivisions of layer 5. A few retrogradely labeled cells could also be found within all of the other layers except layer 1. The only consistent difference seen in the patterns of label following injections centered within CO blobs and interblobs was that cells were always labeled in 4α (4Cα) following injections centered in CO blobs but not following injections centered within interblobs.

Connections of Layer 3A

A total of 18 injections were made into layer 3A, including seven which were restricted to layer 3A. Eleven were located above a CO blob, six above an interblob and in one injection CO blob boundaries were unclear. As we and others reported for other primates (Lachica *et al.*, 1992, 1993; Yoshioka *et al.*, 1994), injections restricted to layer 3A in the owl monkey result in no retrogradely labeled cells within any subdivisions of layer 4 (4C). Figure 11 shows examples from two experiments in which BDA or biocytin was injected into layer 3A and, although numerous axons can be seen traversing layer 4 (4C), no cells in layer 4 (4C) appear labeled. Strong reciprocal connections with layer 5 were consistently observed, however. Interestingly, both the

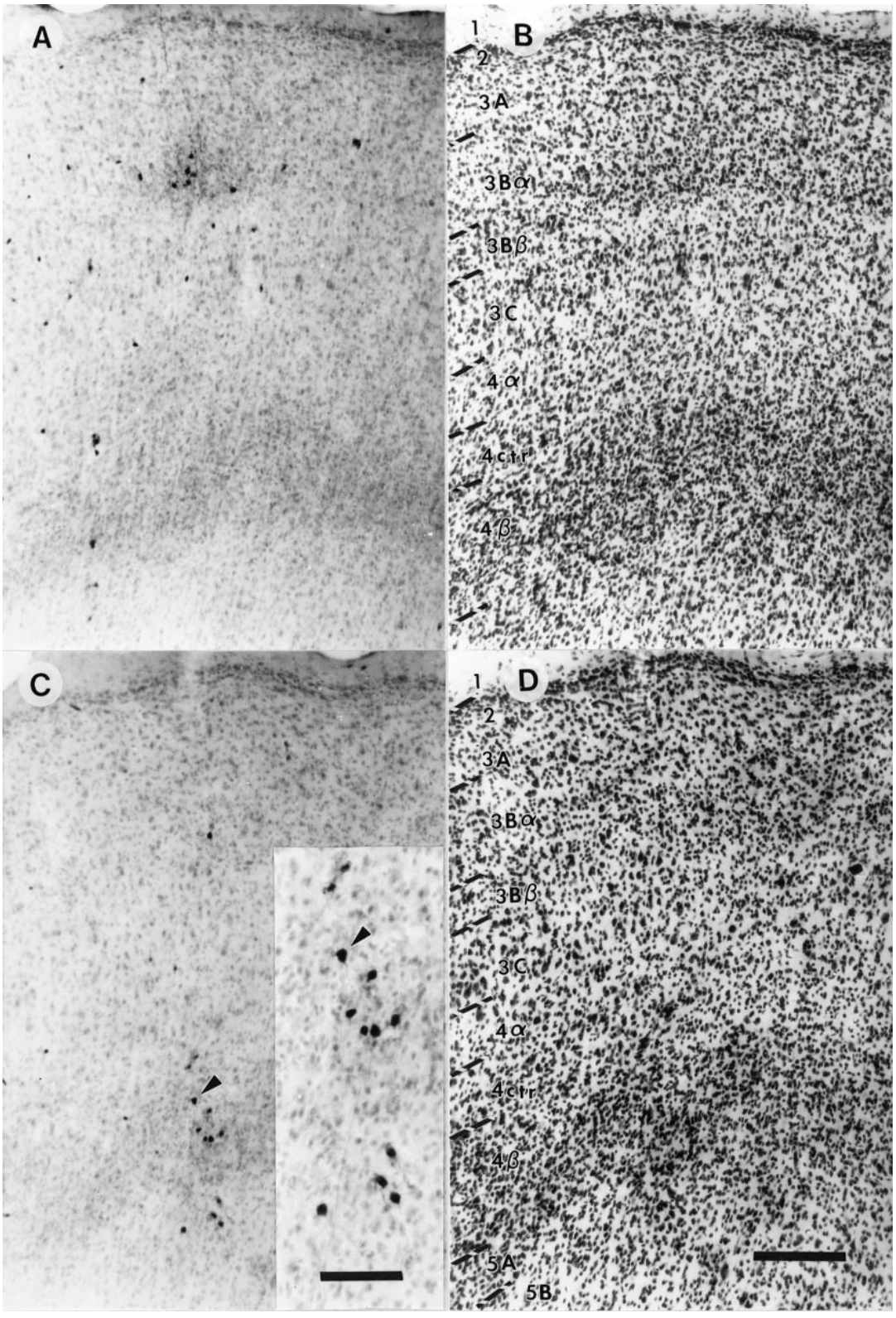

Figure 6. An example of an injection located beneath an interblob in layer 3Bβ (4A). (*A,B*) The same section photographed with a blue filter (*A*) to show the biocytin injection site and without the filter (*B*) to show the Nissl stained laminar pattern. (*C,D*) An adjacent section photographed with and without the blue filter, to show the labeling in layers 4β (4Cβ) and 5A. Note that the retrogradely labeled cells (inset at higher magnification in *C*) are almost entirely confined to layers 4β (4Cβ) and 5B. The arrowheads in (*C*) and the inset point to the same cell. Other conventions as in Figure 1. Scale bar = 250 μm, inset = 50 μm.

anterograde and retrograde labeling were confined to layer 5B, leaving layer 5A as a conspicuously unlabeled cleft between the layer 5B labeling and layer 4. This cleft can be seen in Figure 11*C*, where the section has been stained with CO, thereby marking the lower border of layer 4.

Layer 3A injections often labeled cells in layer 3C (4B). Figure

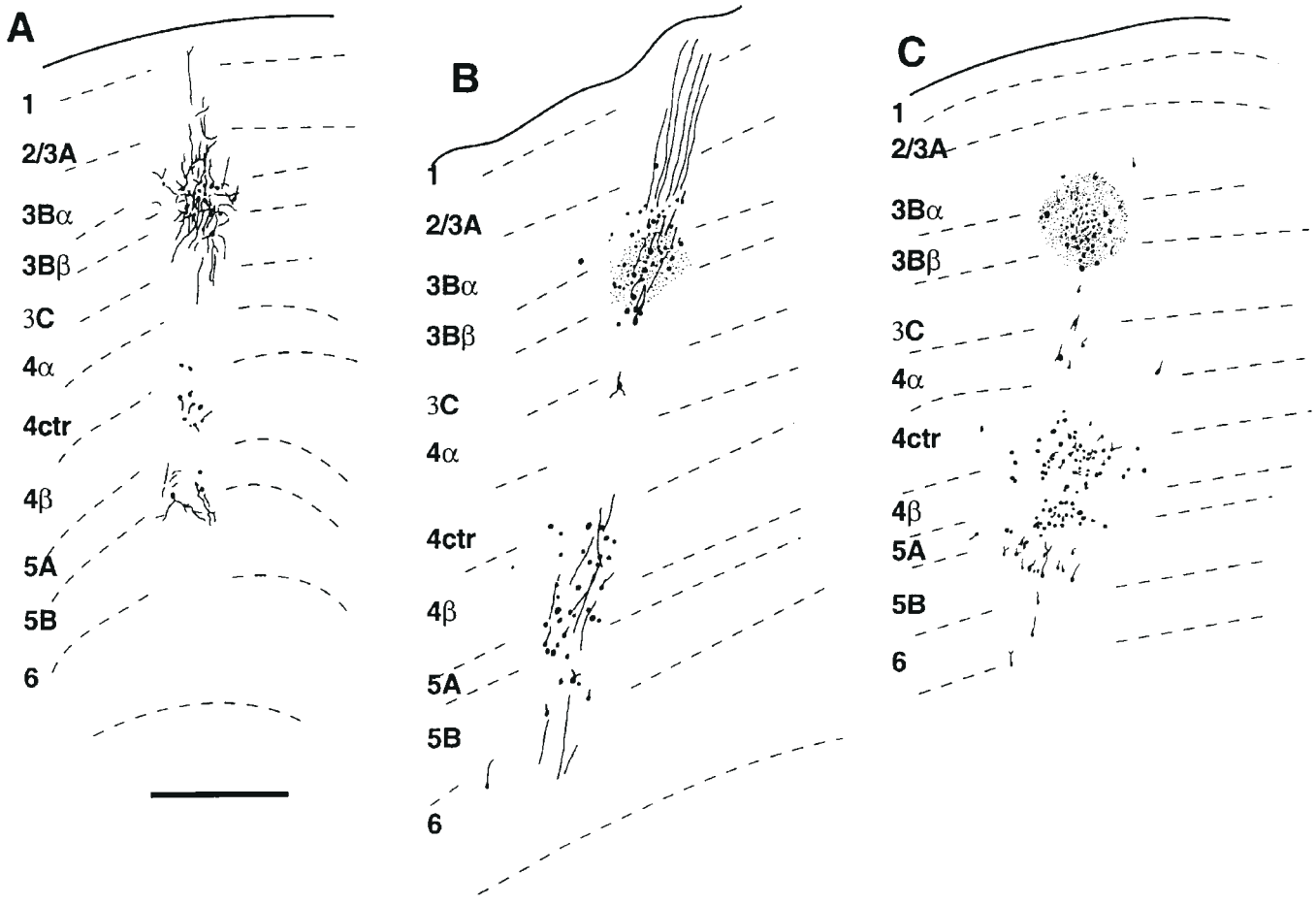

Figure 7. Reconstructions of 3Bβ (4A) injections. (*A*,*B*) Biocytin injections. (*C*) A CTB-Au injection. The injections in (*A*) and (*B*) were confined to layer 3Bβ (4A); the retrograde label in these cases is almost entirely confined to layers 4β (4Cβ) and 5. In the other case, shown in (*C*), the injection was centered on 3Bβ (4A), but encroached on layers 3C (4B) and 3Bα (3B), giving rise to a few labeled cells in 4α (4Cα) and 4ctr in addition to the main focus of labeling in 4β (4Cβ). Other conventions are as in Figure 6. Scale bar = 250 μm.

12 shows reconstructions from three 3A injections, two of which were centered over blobs, the other being centered over an interblob. The second injection is the same as the injection shown in Figure 11*A*,*B*. In both cases, a few well-labeled cells were found in layer 3C (4B). Labeled cells were consistently seen in layer 3Bα (3B) and sometimes in 3Bβ (4A), but the proximity of layer 3Bα (3B) to the injection sites in layer 3A makes it impossible to determine if cells labeled in this layer represent true axonal connectivity.

Discussion

In this paper, we examined the intrinsic interlaminar connections in owl monkey visual cortex, with a special emphasis on the projections from layer 4 to layer 3. Our most significant finding was that layer 4 can be divided into three tiers [4α (4Cα), 4β (4Cβ) and 4ctr] based upon projections to the superficial layers. Specifically, we find that 4α (4Cα), 4β (4Cβ) and 4ctr send primary projections to layers 3C (4B), 3Bβ (4A) and 3Bα (3B), respectively. Cortical layers above layer 3Bα (3B) (e.g. layers 3A, 2 and 1) do not receive any direct connections from layer 4 (4C). Some differences were also observed between the connections of different subdivisions of layer 3 with the infragranular layers, although no consistent differences in connections were seen that distinguished CO blobs from interblobs.

How Many Sublayers Does Layer 4 Have?

The data on the connectivity of layer 4 (4C) described in this study is best explained in a lamination scheme where layer 4 (4C) is divided into three sublayers. Although it has become customary to divide layer 4 (4C) of primates into two sublayers (α and β), there is evidence that two sublayers are not sufficient to accurately describe this layer. Indeed, the upper border of what Brodmann originally defined based upon Nissl stains as layer 4Cα has shifted as studies have come to rely more and more on CO stains. When detailed studies of the geniculocortical innervation of layer 4 based upon intracellular transport of tracers (Hubel and Wiesel, 1972; Hendrickson *et al.*, 1978) were initially made, it was recognized that CO staining showed sites of geniculate termination (Horton and Hubel, 1981; Livingstone and Hubel, 1982) [for a review see (Wong-Riley, 1994)]. Accordingly, the upper boundary of layer 4 was moved upward to correspond to the upper boundary of CO staining and, hence, geniculate input (Blasdel and Lund, 1983). Brodmann's layer 4C was thus expanded at the expense of his layer 4B. Yet, most studies still tended to divide this newly expanded layer 4C into roughly equal α and β divisions, causing a shift in the borders of the originally defined sublayers.

At first glance, the laminar scheme, based upon LGN inputs in which 4α (4Cα) corresponds to the input zone of M fibers and 4β (4Cβ) corresponds to the input zone of P fibers, offers a

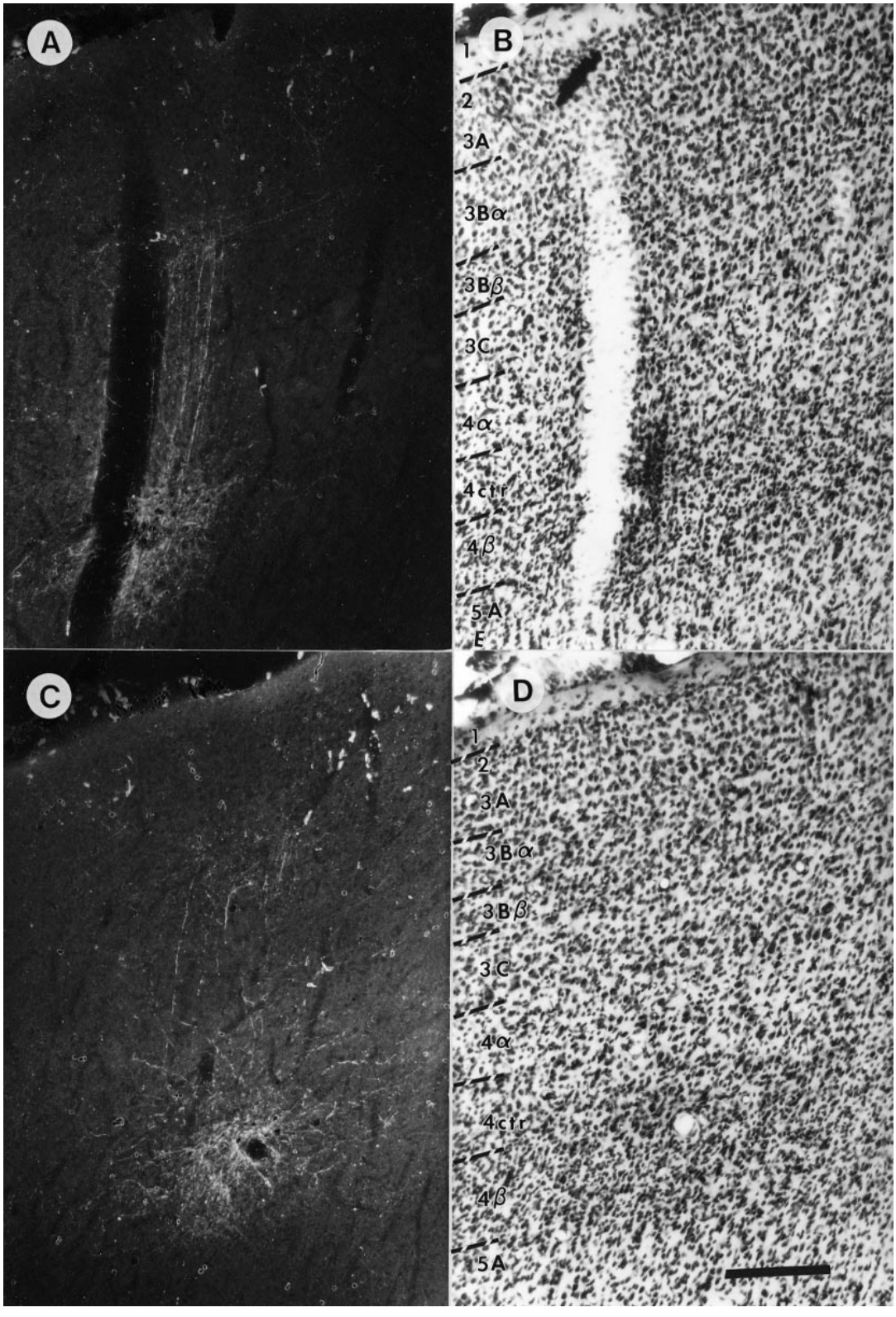

Figure 8. Photomicrographs of anterograde labeling following a biocytin injection within layer 4β (4Cβ). (*A*,*C*) Adjacent sections through the injection site photographed under darkfield illumination. Note the axons ascend from the injection site and terminate within layer 3Bβ (4A). (*B*,*D*) The same sections as shown in (*A*) and (*C*), counterstained to reveal the layers (indicated with Arabic numerals). Scale bar = 250 μm.

more precise way to subdivide layer 4 into the pre-ordained two sublayers. Thus, the layer we define as 4ctr could be assigned to 4α (4Cα) or 4β (4Cβ) based on whether it receives M or P input. However, our results (Fig. 2) show that the pattern of geniculate inputs is, if anything, clearer in dividing layer 4 (4C) into three sublayers than into two. In previous studies, a zone in the center

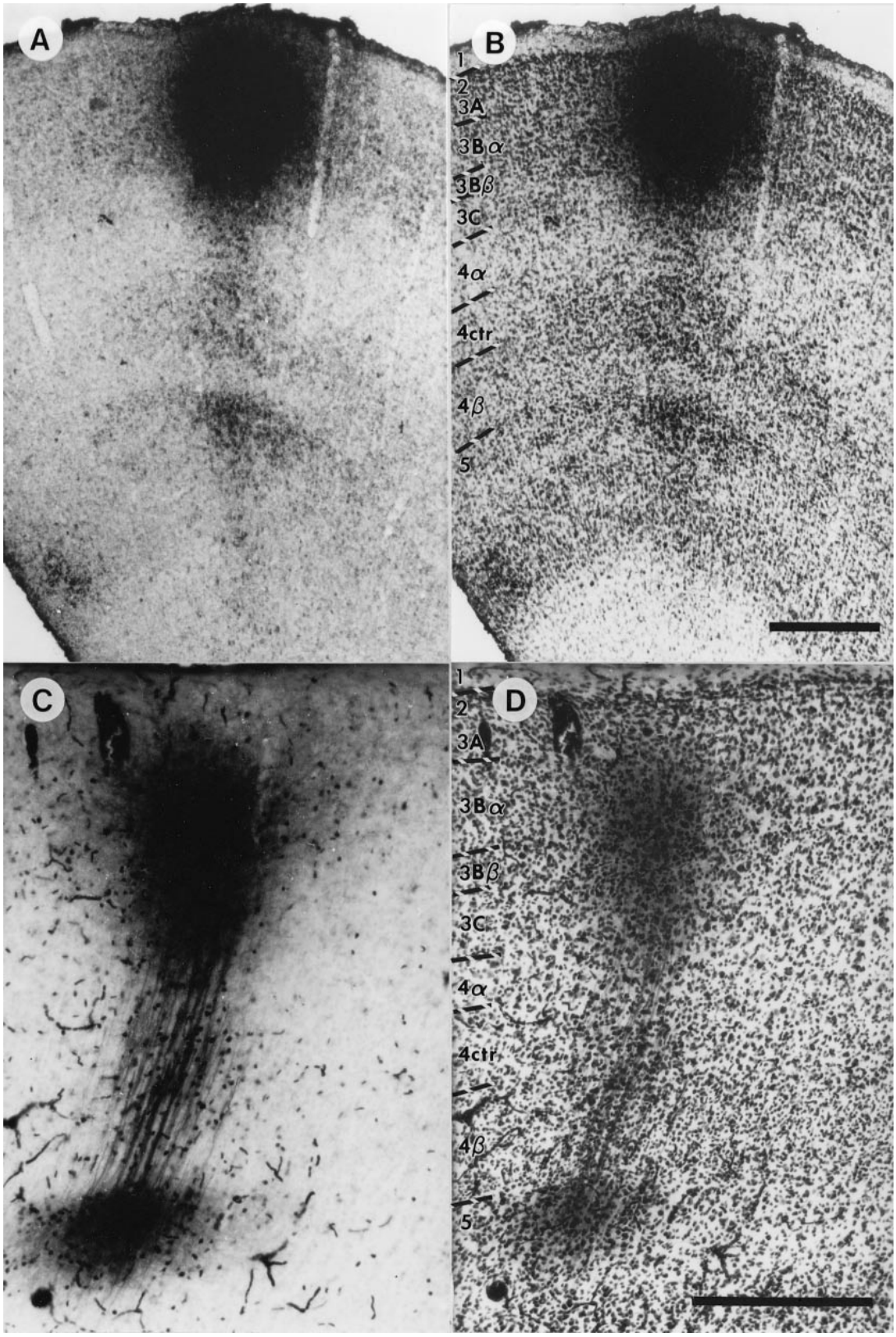

Figure 9. Two examples of injections within layer 3Bα (3B) one in a CO blob (*A*,*B*) and one within an interblob (*C*,*D*). (*A*,*B*) (CTB-Au injection) and (*C*,*D*) (HRP injection) show the same sections photographed with a blue filter (*A*,*C*) to show the injection sites and without the filter (*B*,*D*) to show the Nissl stained laminar patterns. Note that the retrogradely labeled cells are most prominent in layers 4ctr and 5 in both cases. Other conventions as in Figure 1. Scale bars in (*A*,*B*) and (*C*,*D*) = 250 μm.

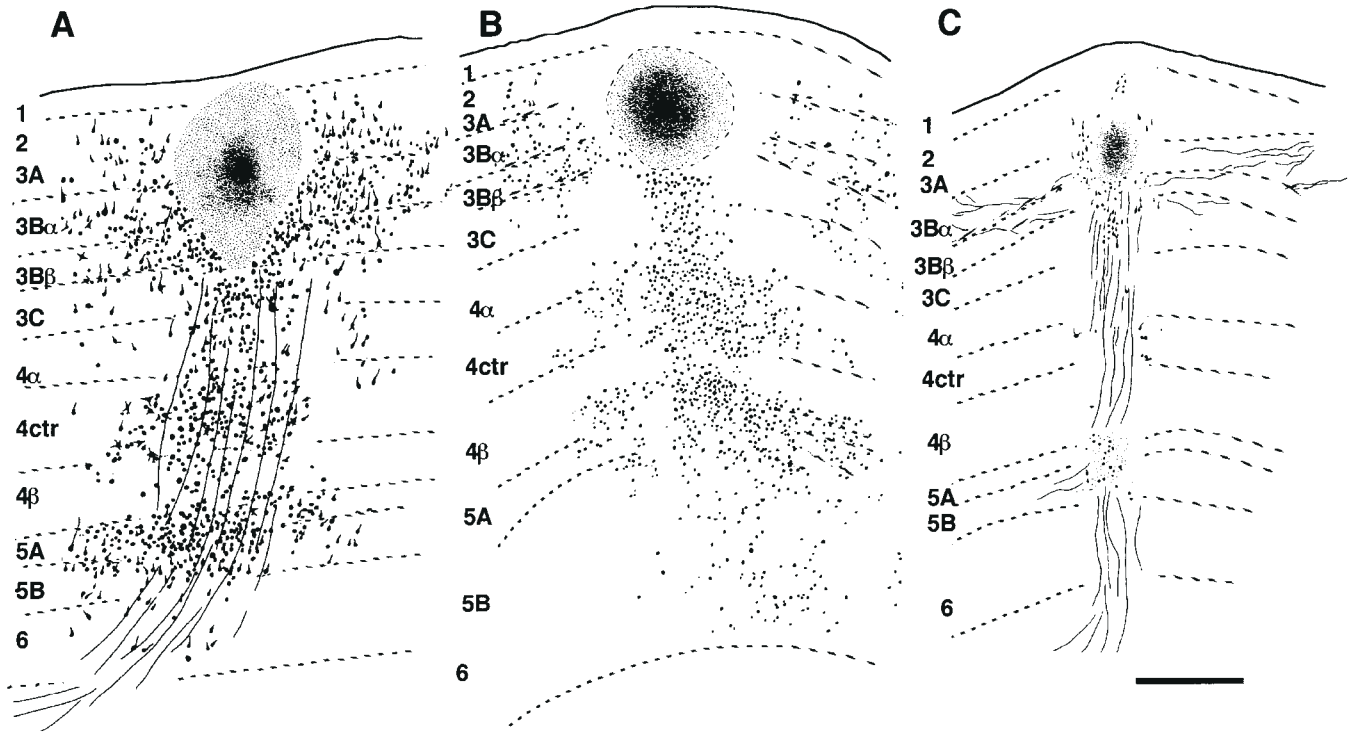

Figure 10. Reconstructions of the distribution of retrograde (large black dots) and anterograde (fine stipple) label following injections within layer 3Bα (3B). (*A*) The retrograde label following a large HRP injection within a CO blob. Labeled cells are seen in all layers except layer 1. Within layer 4 the majority of the labeled cells are found in 4ctr. (*B*) An example of a CTB-Au injection site within a CO blob. As in (*A*), the majority of label in layer 4 is found in 4ctr. (*C*) A restricted biocytin injection located within an interblob. Retrograde label is confined almost entirely to layers 3Bβ (4A), 4ctr, and 5. Other conventions are as in Figure 6. Scale bar = 250 μm.

of layer 4 receiving reduced geniculate input was shown in figure 13 of Fitzpatrick *et al.* (Fitzpatrick *et al.*, 1983) for squirrel monkey V1 and in figure 9 of Katz *et al.* (Katz *et al.*, 1989) for macaque monkey. The question of whether 4ctr receives primarily M or P is not clear at this time. Comparison of published data from bulk tracing experiments suggests that the proportion of M versus P input to layer 4ctr might vary across species, being weighted more towards M input in the owl monkey (Diamond *et al.*, 1985) and more towards P input in macaque (Hubel and Wiesel, 1972) and squirrel monkey (Fitzpatrick *et al.*, 1983).

Blasdel and Lund (Blasdel and Lund, 1983) and Freund *et al.* (Freund *et al.*, 1989) found two classes of M axons terminating in layer 4α (4Cα). The majority of axons arborized throughout layer 4α (4Cα), with minor or no collateral input to layer 6, while the arborizations of the others were restricted to the upper half of layer 4α (4Cα), with extensive collaterals in layer 6. It was later theorized that differences in receptive field sizes and contrast sensitivities in these two populations could account for changes in these properties with depth in layer 4 (4C) (Lund *et al.*, 1995; Bauer *et al.*, 1999). It is possible that the termination zones of these two types of axons correspond to layer 4α (4Cα) and 4ctr as defined in this study; any differences in the LGN pathway projections to the three sublayers of layer 4 (4C) then would be propagated onto different sublayers of layer 3 by the projections shown in this study.

In the present study the projections from 4ctr were found to be different from those arising from 4α (4Cα) or 4β (4Cβ). Specifically, layer 4ctr was the only subdivision of layer 4 (4C) to be strongly labeled after injections into layer 3Bα (3B). That the middle of layer 4 (4C) may have different connections has been suggested in previous studies in other species. Based on retrograde tracing studies in macaque monkey, Fitzpatrick *et al.* (Fitzpatrick *et al.*, 1985) suggested that '. . . the lower half of 4Cβ contributes the bulk of its projection to the dense patchy zone of lamina 4A, whereas the upper half distributes its axons more widely in lamina 3B'. If we equate our 4ctr and 4β (4Cβ) with their upper and lower halves of 4Cβ, then our results in this respect are quite similar to theirs. A striking example of labeling clustered into the center of layer 4 (4C) in squirrel monkey is found in figure 8 of Lachica *et al.* (Lachica *et al.*, 1993). Here, the authors' decision was to draw a single line straight through the center of the labeling and assign half of it to layer 4α (4Cα) and half to layer 4β (4Cβ). Additionally, data from reconstructions of intracellularly labeled cells show a population of neurons in 'lower layer 4Cα' (probably equivalent to our layer 4ctr) with strong projections to layer 3Bα (3B) (Yabuta and Callaway, 1998). Yoshioka *et al.* described labeling of cells in the center of layer 4 (4C) following layer 3Bα (3B) injections, and suggested that this population of cells might receive both M and P input (Yoshioka *et al.*, 1994). Future studies of M and P inputs and their relationship to layer 4ctr might help resolve this question.

Because the studies discussed above did not divide layer 4 (4C) cytoarchitectonically, it is not certain that the differences in connectivity of the center part of layer 4 (4C) described in other species actually correspond to the cytoarchitectonically defined layer 4ctr we describe in the owl monkey in this paper. To address this issue, we re-examined material from this laboratory's previous studies on interlaminar connections in macaque and squirrel monkeys (Lachica *et al.*, 1992, 1993). Figure 13 shows labeling in the middle part of layer 4 (4C) from injections centered in layer 3Bα (3B) in a macaque monkey (*A*,*B*) and a squirrel monkey (*C*,*D*). When the position of the labeling is

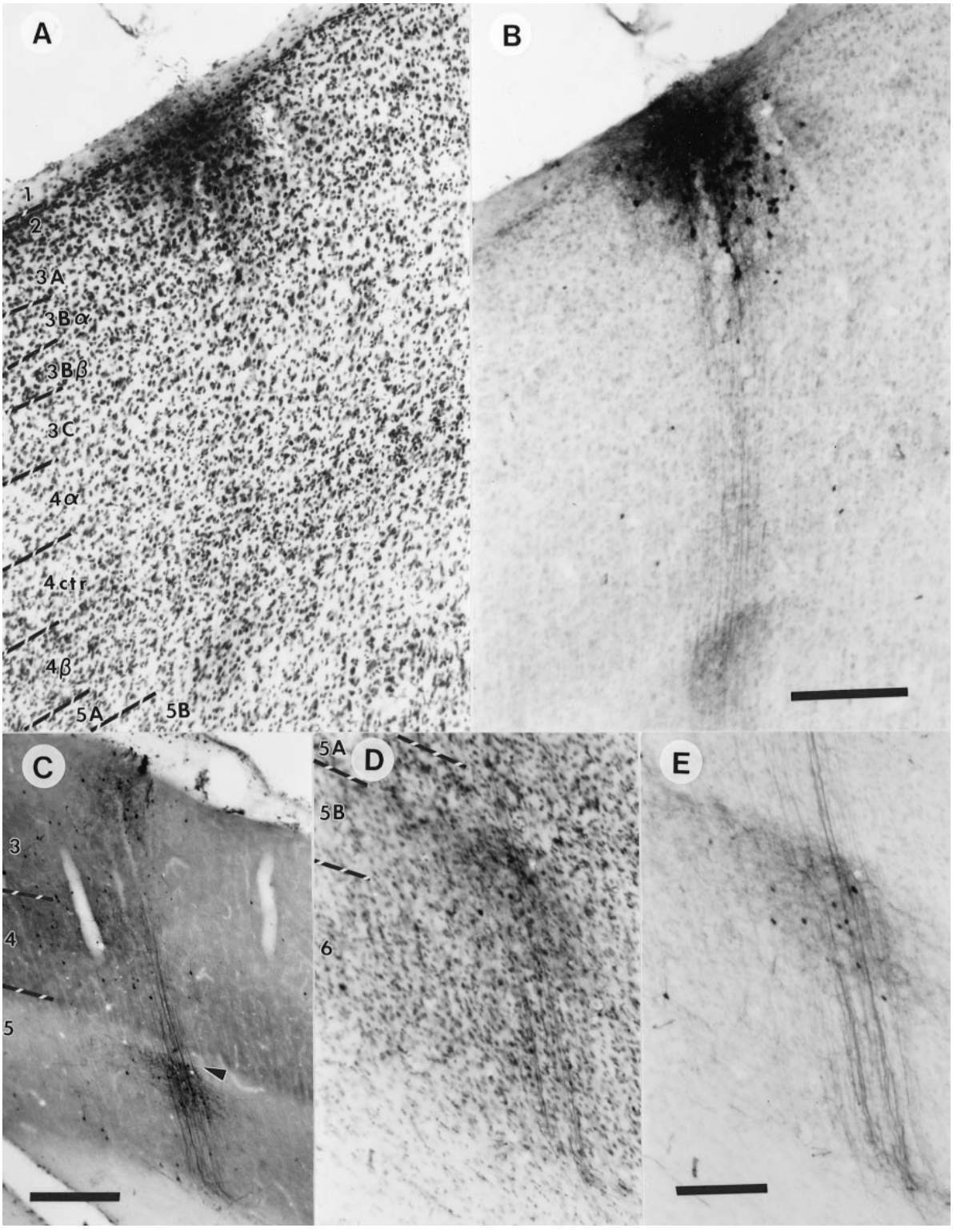

Figure 11. Examples of injections within layer 3A. (*A*,*B*) The same biocytin-reacted section photographed with either a blue filter (*B*) to show the label or without the filter (*A*) to show the layers in Nissl stain. Note that anterograde and retrograde label is almost entirely confined to layer 5B. The absence of labeling in layer 5A is shown clearly in a section from another experiment with BDA (*C*) which was counterstained for cytochrome oxidase. The arrowhead points to the unlabeled cleft that corresponds to layer 5A. Higher power views of an adjacent section stained for Nissl are shown in *D* and *E*. Other conventions as in Figure 1. Scale bars: (*A*,*B*) = 250 μm; (*C*) = 300 μm; (*D*,*E*) = 150 μm.

compared with the three subdivisions of layer 4 (4C) defined by Nissl staining, the labeling is aligned with layer 4ctr. Thus, the definition of layer 4ctr as a cytoarchitectonically distinct subdivision of layer 4 (4C) with a distinct pattern of connectivity relative to layers 4α (4Cα) and 4β (4Cβ) is not unique to the owl monkey, but is found in other primates as well.

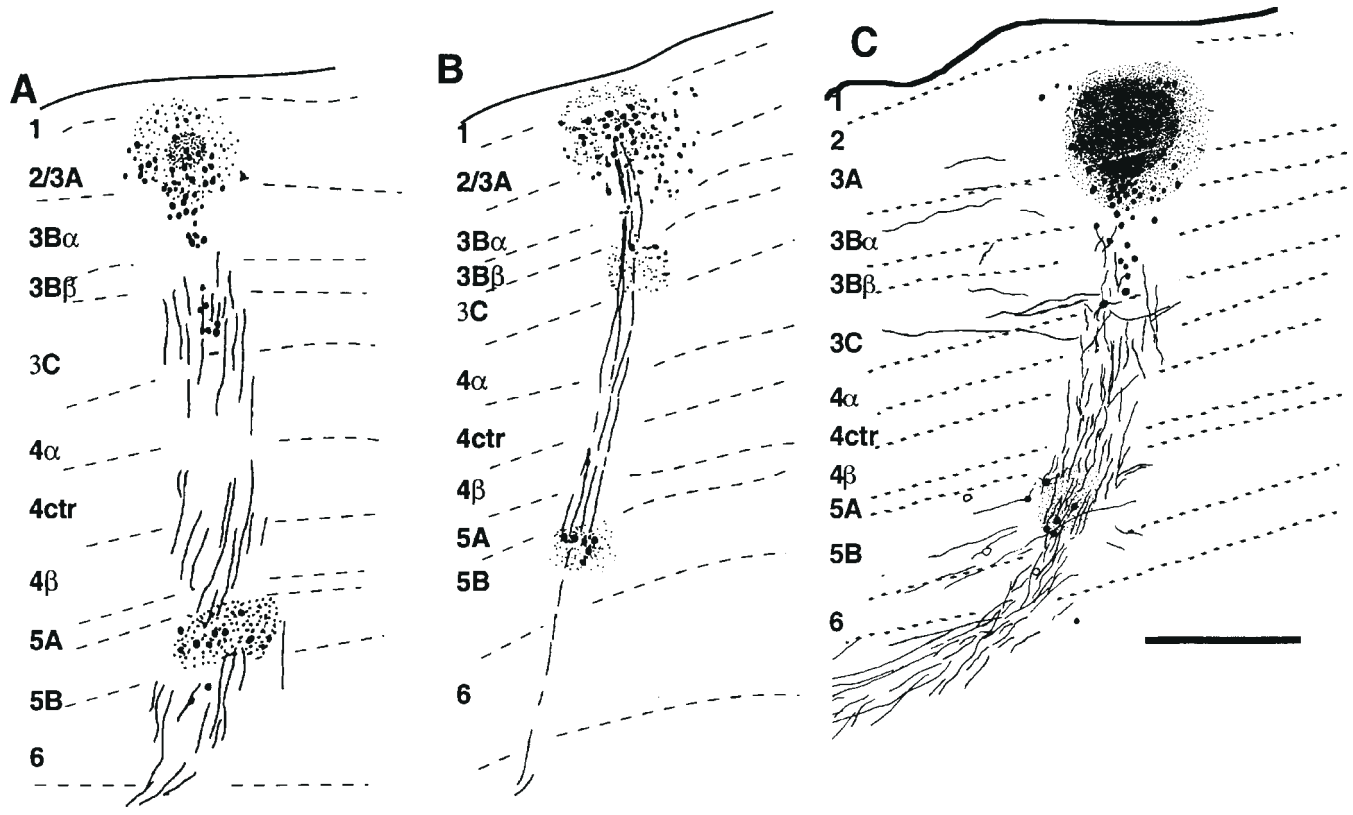

Figure 12. Reconstructions of the distribution of retrograde (large black dots) and anterograde (fine stipple) label following small biocytin (*A*,*B*) or HRP (*C*) injections within layer 3A above a CO blob (*A*,*C*) and an interblob (*B*). Retrograde and anterograde label is confined to layers 3Bα (3B), 3C (4B) and 5B; no labeled cells are found in layer 4. Scale bar = 250 μm.

Species Comparisons

We hypothesized that layer 3Bβ (4A) in the owl monkey might have unique interlaminar connections due to this primate's nocturnal niche, and to its lack of geniculate input to layer 3Bβ (4A). In macaque monkeys, both layer 4β (4Cβ) and layer 3Bβ (4A) display color selectivity (Blasdel and Fitzpatrick, 1984), suggesting that the strong projection between these two sublayers may be due to the fact that they are both processing similar information. Differences in the connectivity in 3Bβ (4A) of the owl monkey might suggest that local cortical circuitry can be modified by changes in inputs. We found instead that the interlaminar connections in owl monkey V1 were very similar to those described in macaque and squirrel monkeys. It is evident that layer 3B in owl monkey V1 can be subdivided in the same way as in macaque and squirrel monkeys, into a lower, smaller celled, more closely packed 3Bβ (4A) receiving strong input from layer 4β (4Cβ) and an upper, larger celled, more loosely packed 3Bα (3B) receiving input from the center of layer 4 (4C). As in other species, the projection from layer 4β (4Cβ) to layer 3Bβ (4A) was one of the most robust projections out of layer 4 (4C). Cortical connections of layer 3Bβ (4A) in the owl monkey are thus similar to those in other primates, although the information these circuits process must be quite different. In this regard, it is noteworthy that apes (e.g. chimpanzees) lack LGN input to 3Bβ (4A) (Tigges and Tigges, 1979) and that humans probably also lack such input based upon CO staining (Horton and Hedley-White, 1984; Wong-Riley *et al.*, 1993), even though 3Bβ (4A) has been described cytoarchitectonically in humans (Yoshioka and Hendry, 1995).

One slight species difference in the projections from layer 4 (4C) that emerged in this study was that, following layer 3C (4B) injections, a variable number of cells were labeled in layer 4ctr in addition to cells labeled in layer 4α (4Cα). This may reflect a different balance of M and P inputs to layer 4ctr of the owl monkey compared with other species. That is, layer 4ctr may be dominated more by M input in owl monkeys than in other species, and this M dominance may be reflected by projections from 4ctr to layer 3C (4B). However, without recognizing a separate layer 4ctr in the earlier studies, it would have been easy to miss the significance of 3C (4B)-projecting cells extending to mid-layer 4 (4C) by assigning these cells to layer 4α (4Cα). Thus, it is not clear if this projection is unique to the owl monkey, or if its recognition in this study is the result of our recognition of layer 4ctr as a separate layer.

The other interesting area of comparison between interlaminar connections in owl monkeys and those of other primate species concerns reported differences between blobs and interblobs. The data of Lachica *et al.* (Lachica *et al.*, 1992, 1993), after compensating for the different laminar designations used in those studies, appear to indicate that while layer 4ctr in the macaque monkey projects to layer 3Bα (3B) in both blob and interblob columns, layer 4α (4Cα) has a projection to layer 3Bα (3B) only in blob columns, with a large projection from 4α (4Cα) to layer 3C (4B) present in both blob and interblob columns. Yoshioka *et al.* confirmed the projection from the middle of layer 4 (4C) to 3Bα (3B) in interblob columns, but they were unable to demonstrate projections from any part of layer 4 (4C) to layer 3Bα (3B) in CO blob columns (Yoshioka *et al.*, 1996). Subse-

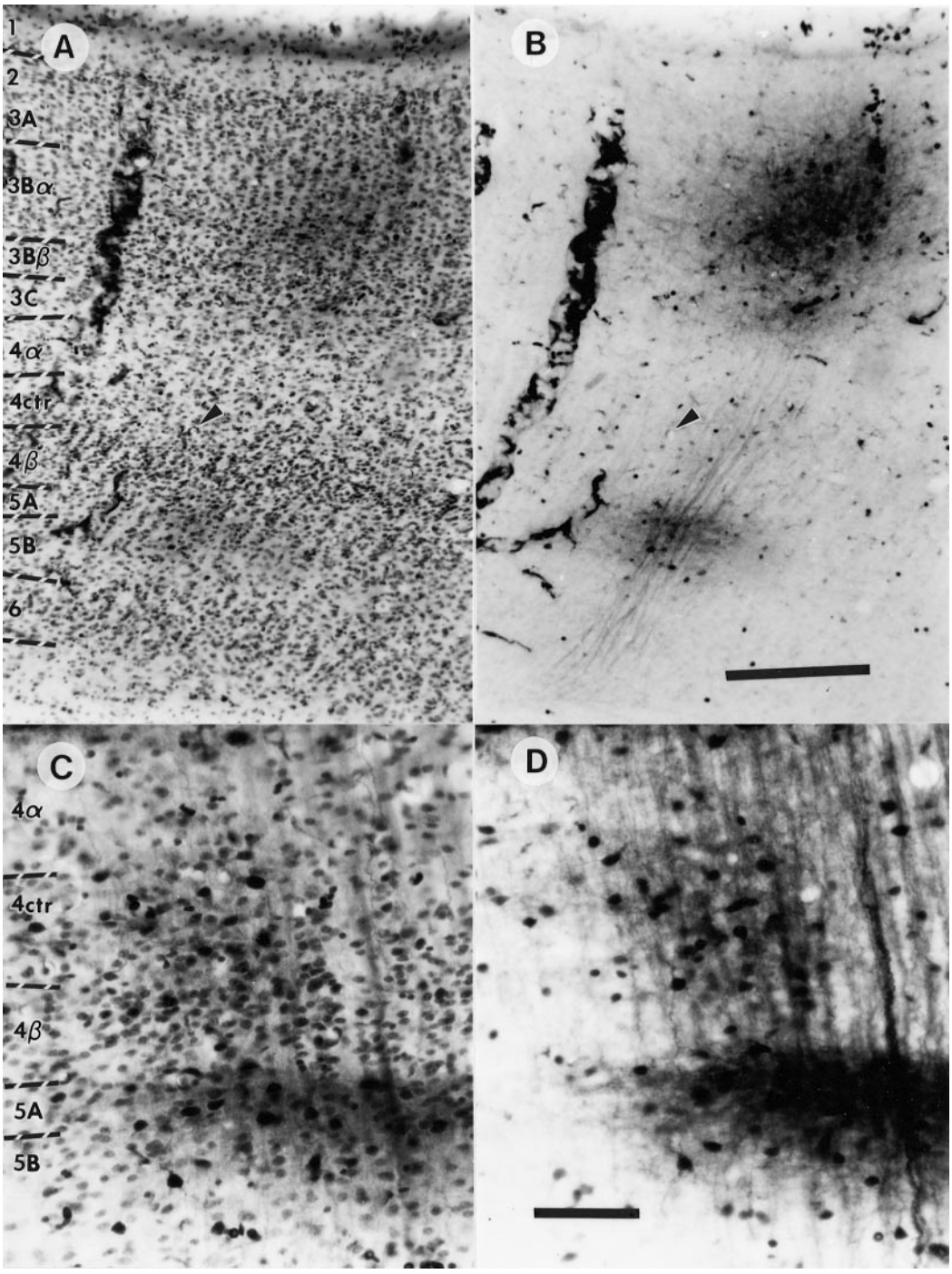

Figure 13. Examples of 4ctr-specific labeling in squirrel monkey (*A*,*B*) and macaque monkey (*C*,*D*) following CO interblob (*A*,*B*) and CO blob (*C*,*D*), HRP (*A*,*B*) or biocytin (*C*,*D*) injections within layer 3Bα (3B). (*B*, *D*) The injection sites photographed through a blue filter to show the label. (*A*,*C*) The same sections as shown in (*B*) and (*D*) photographed without the blue filter to reveal the layers (indicated with Arabic numerals). When compared with the Nissl stain, it is clear in both cases that the majority of retrograde label in layer 4 lies within 4ctr. In (*A*,*B*), label is also apparent in layers 3A, 3C (4B), 4β (4Cβ), and 5. Arrowheads in (*A*) and (*B*) indicate the same blood vessel. In (*C*,*D*) the majority of retrograde label lies in 4ctr, with some label also apparent in layers 4β (4Cβ) and 4α (4Cα), as well as dense label in layer 5. Scale bars: (*A*,*B*) = 300 μm; (*C*,*D*) = 50 μm.

quent intracellular filling studies (Callaway and Wiser, 1996; Yabuta and Callaway, 1998) showed significant input from the center part of layer 4 (4C) to 3Bα (3B) in both blob and interblob columns in macaque monkeys. The data for the owl monkey clearly show that the projection from layer 4ctr to layer 3Bα (3B) exists below both blobs and interblobs. Differences in projection from layer 4α (4Cα) to 3Bα (3B) blobs versus interblobs were more difficult to discriminate; it is hard to say with certainty whether layer 4α (4Cα) has a stronger projection to layer 3Bα (3B) blobs or interblobs in owl monkey V1.

Functional Conclusions

One of the main conclusions that comes out of this study of interlaminar connections is that each of the three sublayers of layer 4 (4C) primarily targets a different sublayer in layer 3. The functional implication of this conclusion is that the partial

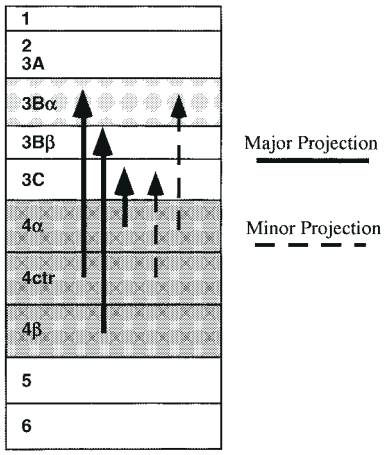

Figure 14. Summary diagram showing projections of layer 4 to layer 3. Layer 4α (4Cα) projects principally to layer 3C (4B), 4β (4Cβ) to 3Bβ (4A), and 4ctr to 3Bα (3B). Layer 3A, the major output layer to area V2, receives signals from layer 4 only indirectly via other subdivisions of layer 3 and layer 5. See text for details.

segregation in layer 4 (4C) of different classes of inputs from the LGN may be continued at the next level of cortical processing in layer 3. It is likely that, while layer 4α (4Cα) is M-dominated and layer 4β (4Cβ) is P-dominated, layer 4ctr is a combination of the two streams. As discussed above, layer 4ctr might be influenced by M cells with lower contrast sensitivity and smaller receptive fields than those M cells which terminate exclusively in layer 4α (4Cα), further functionally differentiating the three sublayers of layer 4 (4C) (Lund *et al.*, 1995). The respective primary targets of 4α (4Cα), 4ctr and 4β (4Cβ) – layer 3C (4B), layer 3Bα (3B) and layer 3Bβ (4A) – might be expected to reflect the differential contributions from the M and P streams (see diagram in Figure 14). Nevertheless, it is important to note that the connections between the three layer 4 (4C) recipient zones [3C (4B), 3Bβ (4A) and 3Bα (3B)] actually may lead to greater mixing between the streams in these sublayers. For example, 3Bβ (4A) projects to 3Bα (3B) (Lachica *et al.*, 1993; Callaway and Wiser, 1996), which would lead to further mixing of M and P input in 3Bα (3B). Additionally, koniocellular (K) LGN axons project directly to the CO blobs within 3Bα (3B), allowing for mixing of all three LGN pathways within these zones (Casagrande, 1994). The intracortical projections from 3Bβ (4A) are of special interest because this layer is the main recipient of P information via layer 4β (4Cβ). However, this layer also gets direct input from collaterals of some K axons in the owl monkey (Ding and Casagrande, 1997), based upon data from single axon reconstructions. In this regard it is also noteworthy that the single axon in the macaque monkey that was reconstructed within 3Bβ (4A) was physiologically identified to be from a blue-ON color selective LGN axon (Blasdel and Lund, 1983); in marmosets and macaque monkeys some K LGN cells have been classified as blue-ON selective (Dacey and Lee, 1994; Martin *et al.*, 1997; White *et al.*, 1998; Solomon *et al.*, 1999). This arrangement would indicate that 3Bβ (4A) is uniquely suited to process color selective information without talking to the M pathway in those species with color vision. However, some cells in layer 3Bβ (4A) project directly to the CO thick (not thin) stripes in V2 of macaque monkeys (Levitt *et al.*, 1994); the CO thick stripes are also the target of input from M dominated layer 3C (4B) (Livingstone and Hubel, 1987; Levitt *et al.*, 1994), providing evidence not only for further mixing of all three channels at the next level, even in species with excellent color vision, but also hinting that cells in 3Bβ (4A) do more than process information about color. If P signals are mixed with other LGN signals from other layers before being relayed out of V1, then there is little possibility for an extrastriate area to receive pure P signals. Contrast this situation with layer 3C (4B), which receives information primarily from the M-recipient layer 4α (4Cα) and acts as the main entry point to the dorsal stream of extrastriate visual areas concerned with visual motion and spatial location (Maunsell, 1987). Even in layer 3C (4B) there is opportunity for contributions from other LGN streams based upon connections between the different sublayers of layer 4. However, unlike P pathway signals, M pathway signals via layer 3C (4B) appear to have much more rapid and direct access to higher order visual areas. This point is reinforced by physiological studies in which M or P LGN input was blocked, which show that the cells in area MT are dominated by M input (Maunsell *et al.*, 1990).

The main output layer to the ventral stream of visual areas concerned with object recognition is layer 3A. Unlike layer 3C (4B), layer 3A is several synapses removed from any direct input from layer 4. As first pointed out by Lachica *et al.* (Lachica *et al.*, 1993), all of the LGN signals received by layer 3A must be filtered through several intracortical relays (with the possible exception of some direct input from LGN K axons). Layer 3A receives projections from layer 3Bα (3B), which in turn receives input from 4ctr, as well as a strong projection from layer 3C (4B) and layer 5 (Lachica *et al.*, 1993; Callaway and Wiser, 1996). It is unlikely, therefore, that any 3A output cells reflect the signature of any LGN pathway in the same way as cells in layer 3C (4B) reflect a strong M input signature. Instead, the connectional arrangement suggests that 3A output cells, unlike 3C (4B) output cells, carry highly processed visual signals appropriate to areas within the ventral stream pathway concerned with complex recognition tasks that are less constrained by temporal factors.

Functional differences have not only been ascribed to V1 layers in primates based upon connections and physiology, but also to the CO blob and interblob compartments (Casagrande and Kaas, 1994). In the owl monkey we did not find major consistent differences in the connections of these compartments. This finding contrasts with our own findings in other primate species (Lachica *et al.*, 1992, 1993) as well as those of others (Callaway and Wiser, 1996; Yoshioka *et al.*, 1996; Yabuta and Callaway, 1998). In the present results there were hints that layer 3Bα (3B) CO blobs receive more projections from cells in layers 3C (4B) and 4α (4Cα) than do layer 3Bα (3B) interblobs; however, the sample size was small. Moreover, with the possible exception of fewer direction selective cells in the CO blobs, no differences were reported in the receptive field properties of cells located within the CO blobs and interblobs of owl monkeys (O'Keefe *et al.*, 1998), even though their CO blobs and interblobs, as in other primates, have different corticocortical connections (Wagor *et al.*, 1975; Krubitzer and Kaas, 1993; Beck and Kaas, 1998). As with our present anatomical data, the physiological data comparing CO blobs and interblobs in owl monkey V1 involves a small sample size. Thus, future studies with larger samples may uncover differences between these compartments that would be expected given their distinct extrastriate projection patterns.

Notes

We are grateful to Drs Edward Lachica, Grant Taylor and Kelly Johnson for help with surgery and data analysis for some of the cases, and to Jennifer Ichida and Amy Wiencken for comments on the manuscript. This research was supported by NIH grants EY01778 (V.A.C.) and core grants EY08126 and HD15052.

Address correspondence to Vivien A. Casagrande, Department of Cell Biology, Vanderbilt University Medical School, MCN C-2310, 1161 21st Avenue South, Nashville, TN 37232-2175, USA. Email: vivien.casagrande@mcmail.vanderbilt.edu.

References

Anderson JC, Martin KAC, Whitteridge D (1993) Form, function, and intracortical projections of neurons in the striate cortex of the monkey *Macacus nemistrina*. Cereb Cortex 3: 412–420.

Bauer U, Scholz M, Levitt JB, Obermayer K, Lund JS (1999) A model for the depth-dependence of receptive field size and contrast sensitivity of cells in layer 4C of macaque striate cortex. Vision Res 39:613–629.

Beck PD, Kaas JH (1998) Cortical connections of the dorsomedial visual area in New World owl monkeys (*Aotus trivirgatus*) and squirrel monkeys (*Saimiri sciureus*). J Comp Neurol 400:18–34.

Billings-Gagliardi S, Chan-Palay V, Palay SL (1974) A review of lamination in area 17 of the visual cortex of *Macaca mulatta*. J Neurocytol 3: 619–629.

Blasdel GG, Fitzpatrick D (1984) Physiological organization of layer 4 in macaque striate cortex. J Neurosci 4:880–895.

Blasdel G, Lund JS (1983) Termination of afferent axons in macaque striate cortex. J Neurosci 3:1389–1413.

Blasdel GG, Lund JS, Fitzpatrick D (1985) Intrinsic connections of macaque striate cortex: axonal projections of cells outside lamina 4C. J Neurosci 5:3350–3369.

Brodmann K (1909) Vergleichende lokalisationlehre der grosshirnrinde in ihren prinzipien dargestelt auf des zellenbaues. Leipzig: J.A. Barth.

Callaway EM, Wiser AK (1996) Contributions of individual layer 2–5 spiny neurons to local circuits in macaque primary visual cortex. Vis Neurosci 13:907–922.

Casagrande VA (1994) A third parallel visual pathway to primate area V1. Trends Neurosci 17:305–310.

Casagrande VA, Kaas JH (1994) The afferent, intrinsic, and efferent connections of primary visual cortex in primates. In: Cerebral Cortex (Peters A, Rockland KS, eds), pp. 201–259. New York: Plenum Press.

Casagrande VA, Taylor, JG, Mavity-Hudson, JA (1992) Intrinsic connections of owl monkey striate cortex: differences between cytochrome oxidase (CO) blobs and interblobs. Soc Neurosci Abstr 18:389.

Cusick CG, Kaas JH (1988) Surface view patterns of intrinsic and extrinsic cortical connections of area 17 in a prosimian primate. Brain Res 458:383–388.

Dacey DM, Lee BB (1994) The 'blue-on' opponent pathway in primate retina originates from a distinct bistratified ganglion cell-type. Nature 367:731–735.

Diamond IT, Conley M, Itoh K, Fitzpatrick D (1985) Laminar organization of geniculocortical projections in *Galago senegalensis* and *Aotus trivirgatus*. J Comp Neurol 242:584–610.

Ding Y, Casagrande VA (1997) The distribution and morphology of LGN K pathway axons within the layers and CO blobs of owl monkey V1. Vis Neurosci 14:691–704.

Fitzpatrick D, Itoh K, Diamond IT (1983) The laminar organization of the lateral geniculate body and the striate cortex in the squirrel monkey (*Saimiri sciureus*). J Neurosci 3:673–702.

Fitzpatrick D, Lund JS, Blasdel GG (1985) Intrinsic connections of macaque striate cortex: afferent and efferent connections of lamina 4C. J Neurosci 5:3329–3349.

Freund TF, Martin KAC, Soltesz I, Somogyi P, Whitteridge D (1989) Arborization pattern and postsynaptic targets of physiologically identified thalamocortical afferents in striate cortex of the macaque monkey. J Comp Neurol 289:315–336.

Hässler R (1967) Comparative anatomy of central visual systems in day- and night-active primates. In: Evolution of the Forebrain (Hassler, R, Stephan, H, eds), pp. 419–434. New York: Plenum Press.

Hendrickson AE (1985) Dots, stripes and columns in monkey visual cortex. Trends Neurosci 8:406–410.

Hendrickson AE, Wilson JR, Ogren MP (1978) Neuroanatomical organization of pathways between the dorsal lateral geniculate nucleus and visual cortex in old world and New World primates. J Comp Neurol 182:123–136.

Horton JC (1984) Cytochrome oxidase patches: a new cytoarchitectonic feature of monkey visual cortex. Phil Trans R Soc Lond B 304:199–253.

Horton JC, Hedley-White ET (1984) Mapping of cytochrome oxidase patches and ocular dominance columns in human visual cortex. Phil Trans R Soc Lond B 304:255–272.

Horton JC, Hubel DH (1981) Regular patchy distribution of cytochrome oxidase staining in primary visual cortex of macaque monkey. Nature 292:762–764.

Hubel DH, Wiesel TN (1972) Laminar and columnar distribution of geniculo-cortical fibers in the macaque monkey. J Comp Neurol 146:421–450.

Jacobs GH, Deegan JFD, Neitz J, Crognale MA, Neitz M (1993) Photopigments and color vision in the nocturnal monkey, *Aotus*. Vision Res 33:1773–83.

Jacobs GH, Neitz M, Neitz J (1996) Mutations in S-cone pigment genes and the absence of colour vision in two species of nocturnal primates. Proc R Soc Lond B 263:705–710.

Kaas JH, Lin C-S, Casagrande V (1976) The relay of ipsilateral and contralateral retinal input from the lateral geniculate nucleus to striate cortex in the owl monkey: a transneuronal transport study. Brain Res 106:371–378.

Katz LC (1989) Local circuits and ocular dominance columns in monkey striate cortex. J Neurosci 9:1389–1399.

Krubitzer LA, Kaas JH (1993) The dorsomedial visual area of owl monkeys: connections, myeloarchitecture, and homologies in other primates. J Comp Neurol 334:497–528.

Lachica EA, Casagrande VA (1992) Direct W-like geniculate projections to the cytochrome oxidase (CO) blobs in primate visual cortex – axon morphology. J Comp Neurol 319:141–158.

Lachica EA, Mavity-Hudson JA, Casagrande VA (1991) Morphological details of primate axons and dendrites revealed by extracellular injection of biocytin: an economic and reliable alternative to PHA-L. Brain Res 564:1–11.

Lachica EA, Beck PD, Casagrande VA (1992) Parallel pathways in macaque monkey striate cortex: anatomically defined columns in layer III. Proc Natl Acad Sci USA 89:3566–3570.

Lachica EA, Beck PD, Casagrande VA (1993) Intrinsic connections of layer-III of striate cortex in squirrel monkey and bush baby – correlations with patterns of cytochrome oxidase. J Comp Neurol 329:163–187.

Levitt JB, Yoshioka T, Lund JS (1994) Intrinsic cortical connections in macaque visual area V2: evidence for interaction between different functional streams. J Comp Neurol 342:551–570.

Livingstone MS, Hubel DH (1982) Thalamic inputs to cytochrome oxidase rich regions in monkey visual cortex. Proc Natl Acad Sci USA 79: 6098–6101.

Livingstone MS, Hubel DH (1984) Anatomy and physiology of a color system in the primate visual cortex. J Neurosci 4:309–356.

Livingstone MS, Hubel DH (1987) Connections between layer 4B of area 17 and the thick cytochrome oxidase stripes of area 18 in the squirrel monkey. J Neurosci 7:3371–3377.

Lund JS, Boothe RG (1975) Interlaminar connections and pyramidal neuron organisation in the visual cortex, area 17, of the macaque monkey. J Comp Neurol 159:305–335.

Lund J, Wu Q, Hadingham PT, Levitt JB (1995) Cells and circuits contributing to functional properties in area V1 of macaque monkey cerebral cortex: bases for neuroanatomically realistic models. J Anat (Lond) 187:563–581.

Martin PR, White AJ, Goodchild AK, Wilder HD, Sefton AE (1997) Evidence that blue-on cells are part of the third geniculocortical pathway in primates. Eur J Neurosci 9:1536–41.

Maunsell JHR (1987) Visual processing in monkey extrastriate cortex. Annu Rev Neurosci 10:363–401.

Maunsell JHR, Neally TA, DePriest DD (1990) Magnocellular and parvocellular contributions to responses in the middle temporal visual area (MT) of the macaque monkey. J Neurosci 10:3323–3334.

O'Keefe LP, Levitt JB, Kiper DC, Shapley RM, Movshon JA (1998) Functional organization of owl monkey lateral geniculate nucleus and visual cortex. J Neurophysiol 80:594–609.

Rockland KS (1992) Laminar distribution of neurons projecting from area V1 to V2 in macaque and squirrel monkeys. Cereb Cortex 2:38–47.

Rockland KS, Pandya DN (1979) Laminar origins and terminations of cortical connections of the occipital lobe in the rhesus monkey. Brain Res 179:3–20.

Solomon SG, White AJ, Martin PR (1999) Temporal contrast sensitivity in the lateral geniculate nucleus of a New World monkey, the marmoset *Callithrix jacchus*. J Physiol (Lond) 517:907–917.

Tago H, McGeer PL, Bruce G, Hersh LB (1987) Distribution of choline

acetyltransferase-containing neurons of the hypothalamus. Brain Res 415:49–62.
Tigges J, Tigges M (1979) Ocular dominance columns in the striate cortex of chimpanzee (*Pan troglodytes*). Brain Res 166:386–390.
Valverde F (1971) Short axon neuronal subsystems in the visual cortex of the monkey. Int J Neurosci 1:181–197.
Wagor E, Lin CS, Kaas JH (1975) Some cortical projections of the dorsomedial visual area (DM) of association cortex in the owl monkey, *Aotus trivirgatus*. J Comp Neurol 163:227–250.
Weber JT, Heurta MF, Kaas JH, Harting JK (1983) The projections of the lateral geniculate nucleus of the squirrel monkey: studies of the interlaminar zones and the S layers. J Comp Neurol 213:113–145.
White AJ, Wilder HD, Goodchild AK, Sefton AJ, Martin PR (1998) Segregation of receptive field properties in the lateral geniculate nucleus of a New-World monkey, the marmoset *Callithrix jacchus*. J Neurophysiol 80:2063–2076.
Wikler KC, Rakic P (1990) Distribution of photoreceptor subtypes in the retina of diurnal and nocturnal primates. J Neurosci 10:3390–3401.
Wong-Riley MT, Hevner RF, Cutlan R, Earnest M, Egan R, Frost J, Nguyen T (1993) Cytochrome oxidase in the human visual cortex: distribution in the developing and the adult brain. Vis Neurosci 10:41–58.
Wong-Riley MTT (1994) Primate visual cortex: dynamic metabolic organization and plasticity revealed by cytochrome oxidase. In: Cerebral Cortex (Peters A, Rockland KS, eds), pp. 141–200. New York: Plenum Press.
Yabuta HN, Callaway EM (1998) Functional streams and local connections of layer 4C neurons in primary visual cortex of the macaque monkey. J Neurosci 18:9489–9499.
Yoshioka T, Hendry SHC (1995) Compartmental organization of layer IVA in human primary visual cortex. J Comp Neurol 359:213–220.
Yoshioka T, Levitt JB, Lund JS (1994) Independence and merger of thalamocortical channels within macaque monkey primary visual cortex: anatomy of interlaminar projections. Vis Neurosci 11: 467–490.
Yoshioka T, Blasdel GG, Levitt JB, Lund JS (1996) Relationship between patterns of intrinsic lateral connectivity, ocular dominance, and cytochrome oxidase-reactive regions in macaque monkey striate cortex. Cereb Cortex 6:297–310.
Zeki SM (1978) The cortical projections of foveal striate cortex in the rhesus monkey. J Physiol 277:227–244.
Zeki S, Shipp S (1988) The functional logic of cortical connections. Nature 335:311–317.